MWANGI, JOSEPH NJOROGE, Ph.D. Ion Mobility Mass Spectrometry of Isomeric RNA Biomarkers. (2018)
Directed by Dr. Norman H.L. Chiu. 85 pp

Ion mobility spectrometry is an analytical technique that separates gaseous ions depending on their mobility in a gas filled cell under the influence of an electric field. More compact ions transit through the cell more easily than elongated ions of the same mass. Ions with a higher charge state also transit faster than those with lower charge states. When coupled to mass spectrometry, which separates ions according to their mass to charge ratios, the synergistic platform becomes a more reliable analytical technique, Ion mobility Mass Spectrometry (IM-MS), which can give an additional information of the samples being analyzed. More importantly, the ability to resolve structural isomers is a very pertinent aspect of this analytical technique. Ribonucleic acid, RNA is one of the two nucleic acids besides Deoxyribonucleic acid, DNA. DNA stores the genetic information of an organism while RNA transfers the genetic information from the DNA for protein synthesis. There are various types of RNAs and most of them, including microRNAs have been reported to be biomarkers for various diseases including cancer. >55 % of the currently reported human microRNAs are isomeric.

Various methods used to analyze microRNAs have their limitations, for mass spectrometry, co-elution from the column of isomeric microRNAs that have close physicochemical properties is a challenge to tandem mass spectrometry. This research focused on developing an ion mobility mass spectrometry-based method geared towards resolving isomeric RNA biomarkers. However, when using ion mobility, scientists are

faced by lack of a universal calibrant which can be applied across platforms and inter-laboratories. In addition, the instrument selected for this study has been reported widely in literature as causing ions to heat up in the ion mobility cell. The first project aimed at addressing the calibration limitation for ion mobility. To address this issue, we have used MALDI (Matrix Assisted Laser Desorption Ionization) matrices to develop a reference method that can potentially be applied across different platforms and in different laboratories using these matrices.

The second project was aimed at investigating the Effects of different modes of operation on total internal energy of ions in traveling wave ion mobility mass spectrometry. We have compared the total internal energy of selected molecular ions as they transit through the Triwave ion mobility mass spectrometry platform by use of percentage dissociation of the ions in the two Collision Induced Dissociation (CID) cells in the instrument when operated in different modes that are available on the platform. These experiments have shed some new insights into the extent of ion heating in the instrument and will be helpful with a project related with the current research in our lab.

ION MOBILITY MASS SPECTROMETRY OF ISOMERIC RNA BIOMARKERS

by

Joseph Njoroge Mwangi

A Dissertation Submitted to
the Faculty of The Graduate School at
The University of North Carolina at Greensboro
in Partial Fulfillment
of the Requirements for the Degree
Doctor of Philosophy

Greensboro
2018

Approved by

_____
Committee Chair

APPROVAL PAGE

This dissertation written by Joseph Njoroge Mwangi has been approved by the following committee of the Faculty of The Graduate School at The University of North Carolina at Greensboro.

Committee Chair _____

Committee Members _____

_____

_____

_____
Date of Acceptance by Committee

_____
Date of Final Oral Examination

TABLE OF CONTENTS

Page

LIST OF TABLES

Page

LIST OF FIGURES

Page

CHAPTER I

INTRODUCTION

1.0 Review of Literature

1.0.1 Nucleic Acids

Nucleic acids store and process genetic information in both prokaryotic and eukaryotic cells, thus the roles they play in cellular processes are vital. The central dogma of biology describes how the genetic information flows from a Deoxyribonucleic acid (DNA) sequence to protein which is the product. Ribonucleic acids (RNAs) is one of the other nucleic acids and the main role of RNA is to carry out the instructions encoded in the DNA for synthesis of proteins. To carry out these complex activities, there are various types of RNAs involved. Generally, the RNAs are grouped into coding and non-coding RNAs. Non-coding RNA is a functional RNA molecule transcribed from DNA but not translated into proteins. They include; lncRNA, miRNA, piRNA and siRNA. Their role is to regulate gene expression. The composition and sequence of canonical nucleotides in addition to their chemical modifications in RNA determine their structures as well as their functions

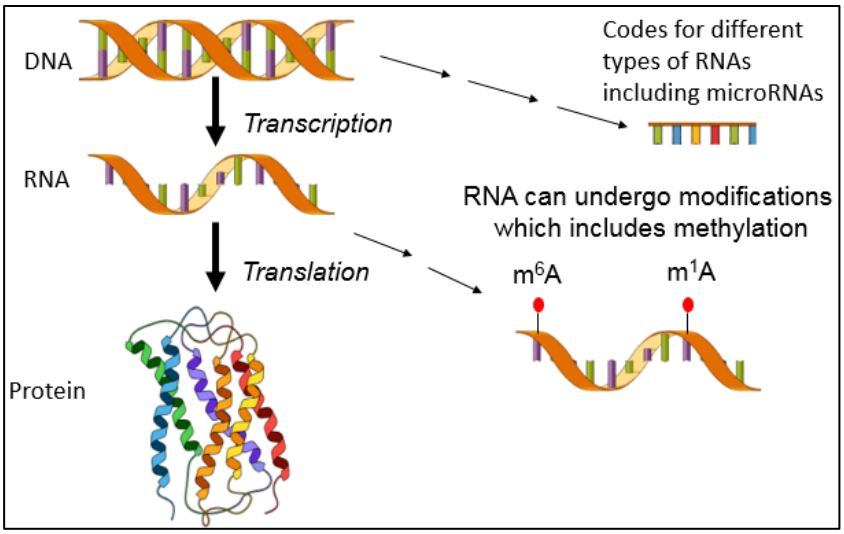

Figure 1.1. Central Dogma of Basic Molecular Biology

1.0.2 MicroRNAs

MicroRNAs are short (18-25 nucleotides, figure 1) non-coding RNAs. They act as main regulators and play a major role in regulation of gene expression through either translational repression or cleavage of mRNA. Due to their roles in various cellular processes, they have been proven to be disease biomarkers for various diseases including cancer. Global profiling of microRNAs will assist in understanding how they carry out these important processes. Thus, having highly sensitive and selective detection methods will assist in extending the insight about their roles especially in human biological processes.

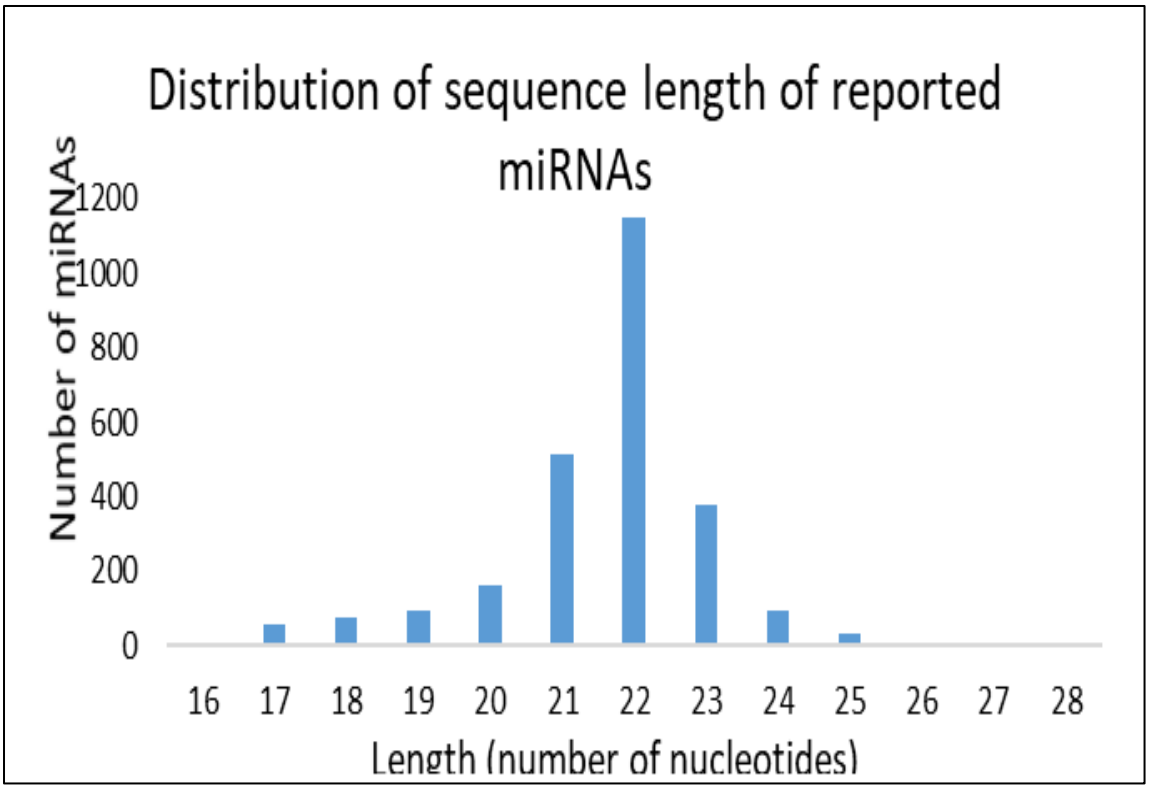

Figure 1.2. Distribution of Sequence Length of Reported Human MicroRNAs

1.1 Challenges of Analyzing MicroRNAs

There are two major challenges that are inherent with microRNAs analysis

1.1.1 Size

They are small in size in comparison to other RNAs, this comes with a challenge to most of the currently applied detection methods which depend on hybridization where a complementary labeled oligonucleotide probe hybridizes with the target microRNA molecule. Small hybridization probes ultimately demand low annealing temperatures which decreases the precision of the probe and thus promoting risks of cross-hybridization. False positive is possible if selectivity is low especially if there is only one mismatch on the base sequence1 between targeted microRNAs and any other available microRNA in the sample.

1.1.2 Low Abundance

The concentration of microRNAs in a cell compared to other RNAs is low, reported to be 0.1%[2]. If isolation of microRNA is the goal, sample preparation and efficiency of the isolation method may limit the sensitivity of the assay. Due to this challenge, microRNA enrichment is needed and this lengthens the assay time.

1.1.3 Isomerism

According to one of our studies, the extent of human microRNAs isomerism is >55%. In addition, some pairs of microRNAs have only one mismatch in their nucleotide sequences. While close similarity in sequence is a challenge to hybridization-based detection methods, using mass spectrometry to analyze a mixture of microRNAs in a sample would prove challenging especially if, due to their similar physicochemical

characteristics, they co-elute from the LC column and will eventually be a challenge to analyze using mass spectrometry alone.

1.2 Established Analytical Methods for MicroRNAs Detection

The existing methods for microRNA detection can be grouped into three main approaches; PCR, Northern blotting and microarray. For all these methods, a transducer must be employed to translate hybridization of the complementary probe to the target microRNA in order for the binding to be picked up as a signal. These methods are briefly discussed here highlighting their limitations.

1.2.1 Reverse Transcription Polymerase Chain Reaction Based Methods (RT-qPCR)

PCR comes in handy when only minute amounts of microRNAs are generated from a sample. Complementary primer oligonucleotides are used to anneal and extend and thus amplify microRNAs in the sample[3]. Because of the short nature of the microRNAs, the primers must be short as well and this, as discussed earlier compromises the sensitivity and selectivity of the method.

1.2.2 Northern Blotting

Considered to be the gold standard for microRNA detection and validation, Northern blotting involves complementary labelled oligonucleotide probe immobilized on a nitrocellulose membrane wells[4] These oligonucleotides have a signal transducer attached to them for signal generation upon hybridization with the target miRNA. The sample containing miRNAs is then added into these wells which is then washed to remove any un-hybridized material. The amount of signal generated from each well is

then measured to account for amount of miRNA present. The limitation inherent with hybridization techniques is a limitation to using this approach.

1.2.3 Microarray

Microarray is known to have a high throughput capability and involves a complementary DNA probe hybridization to a target miRNA. However, instead of labeling the probe, the target microRNA is labelled. This limits hybridization of the target microRNA to an immobilized spot thus making it easy to visualize the process. In addition to hybridization based limitation, microarray is considered to be semi-quantitatively and is limited to comparing expression levels of miRNAs between different samples requiring another method for validation. Since all the miRNAs are analyzed in parallel, it requires the same hybridization conditions, microRNAs have come with a relatively wide range of T_m, it is usually problematic to design probes which will match this requirement[5]. Since microarray requires minimal volume, they are known to have low sensitivity.

1.2.4 Next-Generation Sequencing (NGS)

This is one of the latest detection methods for microRNAs and comes with its own advantages and limitations. It involves ligating sequence adapters to size selected RNA molecules followed by reverse transcription to cDNA. The cDNA is profiled for microRNA fragments with ligated adapter for further sequencing. Since it does not require prior knowledge of sequences, it comes with the potential of discovering novel miRNAs. Also, it generates a huge amount of data depending on the sample. As a downside, high level of computation and validation is required in distinguishing between

real data and noise. NGS requires large amount of RNA sample to prepare the library. Sequence similarity of miRNAs poses to NGS a challenge when discriminating between miRNAs due to PCR and sequencing errors. The short nature of microRNAs and their variable length reduces the ability to accurately identify the border between the miRNA and the adaptor employed [6].

As the technologies discussed above continues to be improved expanding the knowledge on mechanism and functions of microRNAs. There exists a common challenge to all of these methods; close similarity of sequences within microRNAs. As the potential for the methods evolve, a need to develop a method that will among other challenges address cross-hybridization will be necessary.

1.3 RNA Modifications

Modification of RNA is the chemical changes that occur in the composition of RNA molecules after synthesis. These changes have the potential to modify RNA function and/or stability.

As of this writing, 170 different types of RNA modifications at specific locations mainly in their nucleobases or the ribose sugar have been reported[7].

1.3.1 Challenges in Structural Analysis of RNA

The chemical changes on RNA molecules are usually facilitated by specific enzymes. Detecting and analyzing these changes in would help in understanding their biological functions. The following methods, are the most common applied in detection of RNA modifications

1.3.2 Reverse-Transcription Based Methods

RNA templates of interest are transcribed in reverse to cDNA using reverse-transcriptases. These cDNA fragments are then separated in gels. This method utilizes the blocking of the reverse transcriptase upon encountering a modification on the RNA template[8]. Among other limitations, this method cannot detect modifications that are close to the ends of the RNA molecule[9]. In addition, not all modifications can cause the reverse transcriptase to stop and therefore some of the modifications are lost or cannot be detected using this method.

1.3.3 Chromatography Based Methods

Liquid chromatography methods are used to identify modified nucleosides based on the differences in their chromatographic retention time compared to the canonical nucleosides. Thin layer chromatography is a relatively simple and simple cost-effective method suitable for small research laboratories. It is usually applied for shorter RNA molecules. Complete digestion using different nucleobases assists in building up of 5'-monophosphate nucleosides or dinucleotide diphosphates maps which show localization of the modifications. Due to close physicochemical characteristics of modified fragments or even nucleosides, possibility of co-elution from the column exists.

1.3.4 Next-Generation Sequencing

NGS provides high throughput capability and opportunities for new applications, but the costs on its equipment's reagents and data analysis may exceed the budgets of many research projects. More importantly, NGS is NOT capable of detecting majority of the chemical and enzymatic modifications on RNA molecules.

1.3.5 Mass Spectrometry Based Methods

To address the issue on the detection of RNA modifications, an alternative method, namely liquid chromatography-mass spectrometry (LC-MS), is commonly used. RNA modifications would usually lead to changes in the molecular mass of RNA, except the isomerization of uridine, thus allowing the use of MS measurements to identify the type of RNA modification[10, 11]. However, some specific RNA modifications could occur at different positions within the same nucleotide, for example N^6-methyladenosine (m^6A) and N^1-methyladenosine (m^1A). In addition, Adenosine can also be methylated at positions 2 and 8 resulting in m^2A and m^8A respectively[12]. It is important to note that all these modifications are isobaric. Thus, the detection of isobaric RNA modifications represents significant analytical challenge. Thus, distribution of these methylations in RNA is poorly understood. MS measurement cannot differentiate these modifications. To overcome this challenge, Jaffrey and his co-workers have recently reported the use of anti-m^6A antibody in detecting m^6A in the whole transcriptome[13]. It is important to note that m^6A antibody also recognizes also recognize N^6,2′-O-dimethyladenosine (m^6Am) and can result in misidentification[14, 15]. The method involves fragmentation of RNAs to sizes between 50 and 100 nucleotides that may or may not consist of methylated RNA.

Following the recognition of m^6A, the immunoprecipitating of the fragments that consist of m^6A was carried out. By using NGS, the approximate position of m^6A within a RNA molecule was determined. This method lacks the ability to generate a signal that corresponds to the direct detection of m^6A, which is often one of the ways to accurately differentiate m^6A from the other possible RNA methylation. More importantly, this

method does not pinpoint the exact location of the modified nucleotide, which is required for studying the subsequent effects of having the RNA modification. Another drawback of this method may include the fragmentation of larger RNAs into shorter fragments may generate isomeric RNA fragments, i.e. same size and identical nucleotide composition, and poses another challenge to the MS measurements.

1.4 Purpose of the Study

The purpose of this study is to develop a new an ion mobility mass spectrometry-based method that can address the analytical challenge in isomeric RNA identification

1.5. Hypothesis and Specific Aims

1.5.1 Hypothesis

We hypothesize that ion mobility mass spectrometry can facilitate the identification and differentiation of isomeric modified and unmodified RNA biomarkers

1.5.2 Specific Aim 1

To utilize intrinsic MALDI matrix cluster ions that coexist with samples as internal reference in Ion mobility Mass Spectrometry

1.5.3 Specific Aim 2

To investigate the extent of cooling/heating of ions in Triwave ion mobility mass spectrometry

1.5.4 Specific Aim 3

Establish the extent of Isomerism in human microRNA disease biomarkers and the inherent analytical challenges

1.6 Significance of the Study

RNA has a crucial role of regulating cellular processes. For RNA to effectively carry out this function in a cellular milieu composed of DNA and proteins, modifications, which sculpts its niche and entrenches its vital role is a necessity. These modifications have been associated with human diseases, for instance, in human, the discovery of fat mass and obesity associated gene (FTO), which oxidatively demethylates m^6A in vitro established a link between methylation of Adenosine to human health. FTO is highly expressed in the brains and located within the hypothalamus, an important part of the brain dedicated to metabolism. Genome wide association studies have found a strong association between FTO and risk of diabetes and obesity in multiple human populations. Unswerving from human data, growth impedance, altered body weight and increased calamitous results were observed in mice upon deletion of FTO gene. Identification and localization of these vital modifications are lost when using high throughput sequencing methods where reverse transcription of RNA into complementary cDNA is performed.

The alternative to these methods are enzymatic or chemical hydrolysis of the RNA which obliterates sequence information of the RNA of interest not to mention the laborious labelling that comes with these methods. Furthermore, none of these methods could identify and locate both modifications simultaneously. Thus, developing a method that will locate the modification site and discriminate between the modification type and location will assist in understanding effects of these modifications at specific genes. In addition, via one of our ongoing research projects that focuses on the detection of

unmodified microRNA, we realized that there is an unexpectedly high percentage of isomeric microRNA within the human body.

Isomeric microRNAs are defined as having the same number of nucleotides and their nucleotide composition are identical. We coined the term SimiR (Structural isomers of microRNAs). There are currently over 2500 human microRNAs reported. More than 55% of these are composed of sequence isomers. Isomerism of such short sequences poses an insurmountable analytical challenge from the perspective of MS measurements since isomeric microRNAs are indistinguishable by their molecular masses alone, unless tandem MS measurements are used, and complete sequence coverage can be achieved. Some isomeric microRNAs could also have a high degree of sequence similarities.

This represents a challenge to the LC separation prior to the MS measurements. In other words, isomeric microRNA could be co-eluted from the LC column. Isomeric microRNAs are encoded by different genes. Some of them are associated separately to the same disease. Hence, it is important to come up with an analytical capability to distinguish isomeric microRNA in the LC-MS methods. Eiichiro et.al.[16] employed Ion mobility mass spectrometry to resolve two isomeric microRNAs which proved futile. In this study we planned to apply both ion mobility and mass spectrometry to come up with a novel method to resolve isomeric RNA. To achieve this goal, we first tackled two underlying challenges that come with the technique and instrument employed to this end. First, we developed a method which uses intrinsic matrix cluster ions, reported as interfering with the low mass range in mass spectrometry, as internal reference for ion

mobility. This method has a potential of being applied across different platforms and laboratories as long as MALDI matrices are co-crystalized with the samples of interest.

The instrument used in this study, Synapt G2, has been reported widely in literature to cause ion heating in the ion mobility cell. Since this was the first time our research group was using the instrument, we embarked on investigating the extent of heating and the effect it would have on our studies. We compared the total internal energy of the ions as they transit through the platform using the percentage of dissociation of the ions in the two CID cells and the two modes operation available in the instrument. The findings reported and discussed in this dissertation (Chapter four) will assist our research group in achieving the goals of a related research project

CHAPTER II

ION MOBILITY MASS SPECTROMETRY

2.1 Ion Mobility Spectrometry

Primers for the gene *prpC* Ion mobility spectrometry is a technique employed in separation of chemical substances as gas phase ions based on their transit in a gas filled compartment under influence of an electric field (E, in units of V/cm). When in presence of an electric field, gas phase ions attain a drift velocity, V_d (cm/sec) which is proportional to the strength of the electric field thereof. Thus, $V_d = KE$

Where K is the mobility constant, E is the electric field strength and of course V_d is the ions drift velocity. Acceleration of the ion by the electric field, E is proportional to the charge of the ion, e. Since elongated ions experience more deceleration than compact ions, the mobility of the ion is inversely proportional to both N (gas number density, (Number of particles of the gas present in a given volume), and the rotationally averaged collision cross section of the ion,Ω. In presence of a buffer gas, the gaseous ions mobility is decelerated by the collision of the buffer gas molecules. Thus, the ions velocity is inversely proportional to the gas number density, N

With a light buffer gas e.g. Helium, detailed structural information of the ions can be gathered by applying an equation that quantifies the mobility of the ions, K with respect to all the preceding quantities usually referred to as, Mason-Schamp equation. Thus

$$\Omega = \frac{3ze}{16N}\left(\frac{2\pi}{\mu k_B T}\right)^{1/2}\frac{1}{K_0} \qquad \text{equation 1}$$

Where K_0 is the reduced mobility measured at standard conditions, E is the elementary charge, Z the charge state of the ion, μ the reduced mass of the buffer gas with (mass M) and the ion with (mass m) i.e. μ=Mm/(M+m), k_B is the Boltzmann constant and T is the buffer gas temperature

Since an ion mobility analyzer requires low power supply, is light in weight and is compact in size, this has enabled its wide application as handheld devices in the field and on-site. It's high sensitivity in a wide range of conditions has played an unprecedented role in chemical weapons monitoring within the military and application in commercial aviation in detection of explosives. The utility of IM is predicated by the ability of chemical substances ease of ionization. The ions hit the detector, are neutralized and the current generated is amplified then Fourier transferred to a read-back which is a mobility spectrum

2.2 History of Ion Mobility

The history of ion mobility can be traced back to when Ernest Rutherford ionized molecules by x-ray, 1897 and later characterized them using their mobilities, in 1899. This was followed later by theoretical studies on ion mobility by Mason & Schamp in 1958 and McDaniel in 1964 which laid the foundation of IM-MS studies as we know it today.

2.3 Ion Mobility Mass Spectrometry

When ion mobility spectrometry is hyphenated with mass spectrometry, hereby referred to as IM-MS, an additional level of information is gained which breeds a synergistic technique capable of discriminating ions based on the mass to charge ratio in addition to the topology of the ions which has enabled it to gain traction in separation of complex samples in metabolomics[17-19] ,glycomics[20] anomers using ion mobility mass and proteomics[21, 22]. This hybrid of complementary analytical techniques has seen a significant progress both in technological advances and in a wide range of pioneering applications. It has pushed the limits of analytical techniques and enabled sufficient delivery of comprehensive sample information. This is evidenced by the increase in the number of publications with ion mobility mass spectrometry as the analytical technique (Figure 2.2). A critical advantage of IM-MS is the ability to discriminate structurally isomeric samples[22-25] (Figure 2. 1) and polymeric isomers[26].

It is predictable that; this technique will continue to gain ground in multidisciplinary areas of science. A variety of IM designs have been described in literature which includes; Drift time[27, 28] Differential[29], Triwave[30] and Trapped ion

mobility spectrometry[31]. The interfacing of these ion mobility spectrometers with different types of mass analyzers i.e. time of flight, ion Trap, ion Cyclotron, magnetic sector and the quadrupole has made it possible to come up with several IM-MS configurations. Traveling wave based ion mobility (TWIMS) is one of the latest novel ion mobility technologies[32] and consists of stacked ring electrodes with adjacent rings having opposite phases of RF voltages which radially confines the ions within the device while a DC potential is applied to a pair of adjacent rings sequentially and in pulses, resulting into a traveling wave where the ions surf the wave with some falling off while others riding with the wave, helping in separation of the ions according to their mobility. The data reported in this study was carried out in a Synapt G2[33], a Waters instrument using triwave technology.

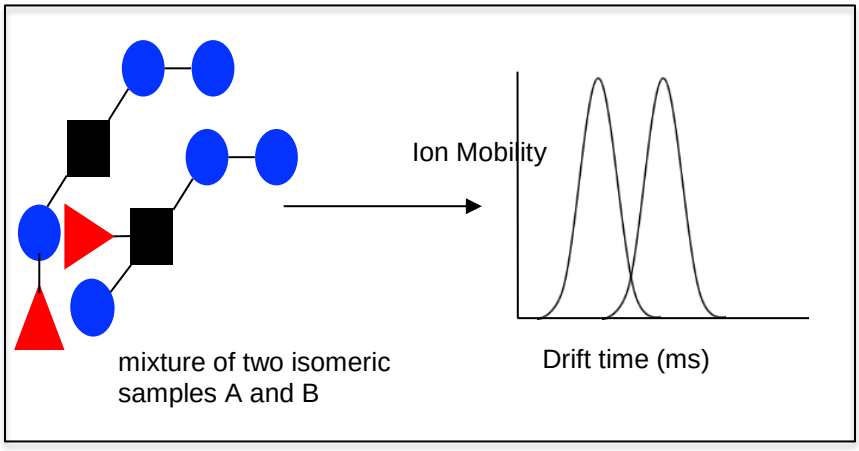

Figure 2.1. Simplified View of what Ion Mobility Separation of Isomers Could Achieve

The figure below is an evidence of how this progress has energized research in varied fields. Data was generated using Web of Science, SCI-expanded between 1992 and 2017, search terms ‘ion mobility’ and ‘mass spectrometry’.

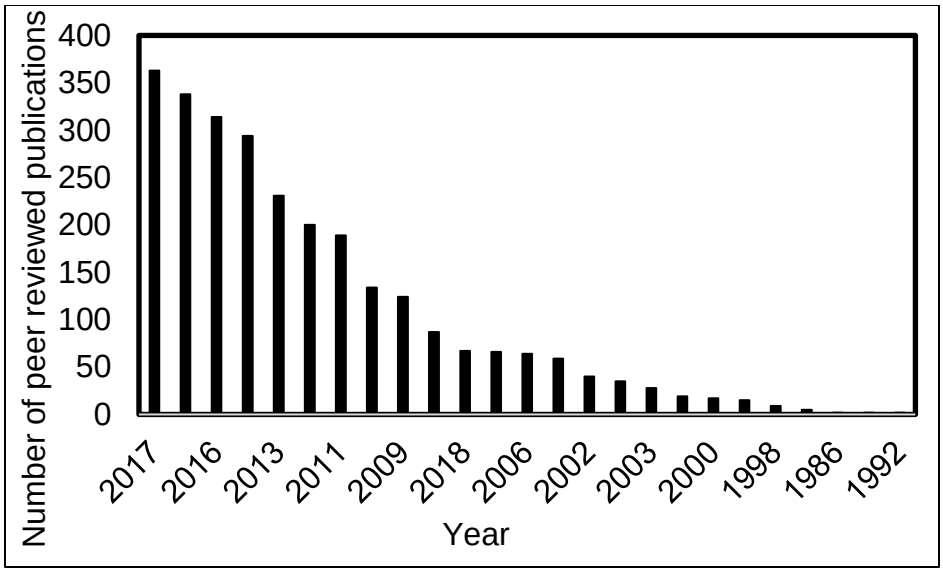

Figure 2.2. Number of Peer-Reviewed Papers Published Annually (to end of 2017) Combining Ion Mobility and Mass Spectrometry

2.4 Commercially Available Ion Mobility Instruments

Different ion mobility technologies have been developed over time with different modes of operation and design. The choice of the type of instrument to apply in analyzing one's sample will depend on availability of funds and the analytical needs of the sample. Although there are various commercially available mass spectrometry instruments to choose from, the number of ion mobility mass spectrometry commercially available do not match up. This could be because the technology and its application is picking up and we could see a surge in the number of these instruments in the near future.

2.5 Triwave Ion Mobility Mass Spectrometry Instruments

Traveling wave technology based ion mobility instrument, Synapt T-Wave SYNAPT G2 HDMS (Waters, U.K.) by Waters was chosen for the study. The unique layout for the components of this instrument made it a great choice for our work. It has

two collision cells, one immediately before the IMS cell, the Trap, and the other immediately after IMS called the Transfer cell. This provides us with the ability to perform two CID or MS/MS (Collision Induced Dissociation) processes either before or after separation in the IMS cell or in both cells. It is also reported to have a high duty cycle[34]. In addition, it has switchable ionization sources i.e. MALDI and ESI at the front. However, one of its downside as widely reported in the literature is that *ion heating occurs in the IMS cell*. The effect of this heating on CID experiments, to our knowledge, has not been reported

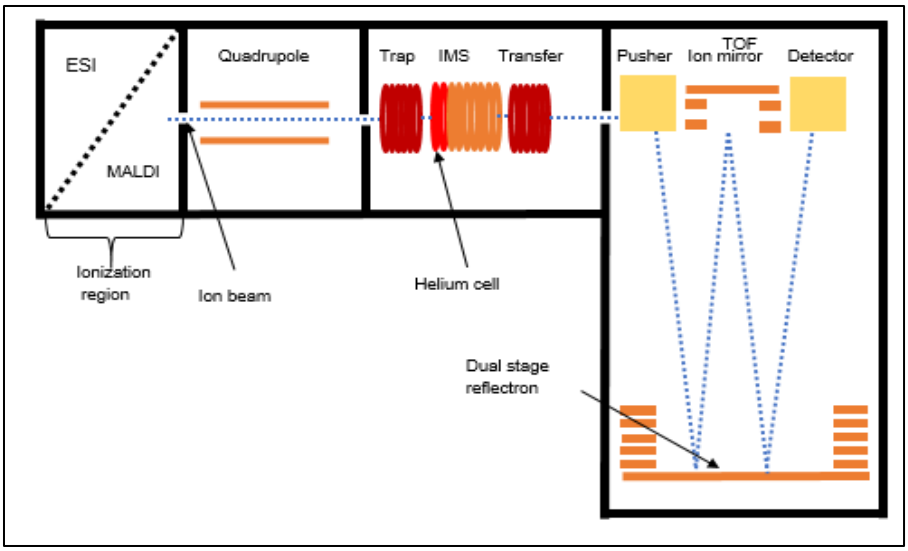

Figure 2.3. The Synapt G2 Schematic Diagram

2.6 Ion Mobility Mass Spectrometry Calibration

Like the conventional MS techniques, success on IM-MS measurements relies on the calibration of both drift time and mass. Unlike in drift tube ion mobility instruments, the golden standard for calibration of traveling wave ion mobility instruments requires experimentally determined collision cross section (CCS) values of well-known calibrants as references[32, 35, 36]. The relationship between CCS and arrival time distribution (t_D) is a well-established theoretical and practical underpinning[37]. Use of a wide variety of calibrants with known collision cross section has been reported[38-40]. These calibrants must meet specific standards including; their CCS values must be accurately reported and published, their size should cover the range of the analytes of interest and they should be rigid enough to withstand potentially harsh sample preparation and experimental conditions e.g. temperature, pressure, humidity and the nature of the drift gas which

could change their conformations in the process. Effects of these conditions on calibrants are minimal when analysis is done under the same conditions and on the same instruments. However, reproducibility is a challenge when experiments are performed across laboratories and in disparate instruments. For the users of travelling wave ion mobility instruments which includes the Synapt series, various researchers have reported a variety of calibrants for specific analytes. For instance, Julien De Winter et.al[41]. have developed synthetic polymers for calibrating the Synapt G2 in positive ion mode only. Structurally different calibrants used usually results in higher error values in CCS measurements[42]. All these reports are born of the fact that there lacks a single calibrant which can be employed for analysis of a wide range of analytes regardless of their structural differences. Thus, *there is a lack of consensus on the choice of universally accepted calibrants* among the IM-MS scientists.

2.7 Conclusion

Commercially available Triwave ion mobility mass spectrometry instrument, Synapt G2 would be a good fit to complete our studies. This is because of the instrument's unique layout that will assist us in combining MS/MS with ion mobility separation. However, a common challenge with ion mobility calibration exists. We endeavored to tackle the calibration challenge that would set a pace for our studies on isomeric modified/unmodified RNA molecules.

CHAPTER III

MALDI MATRIX CLUSTER IONS: INTERNAL REFERENCE IN ION MOBILITY

3.1 Introduction

Matrix Assisted Laser Desorption Ionization (MALDI) is an ionization technique widely applied in analysis of both biomolecules and synthetic polymers. A specific MALDI matrix selected to assist in ionizing the analyte of interest is desorbed in a plume, usually in-vacuo and in the process, the analyte is ionized producing predominantly singly charged ions. MALDI matrix cluster ions are known to interfere with the interpretation of the analyte peaks in the low mass range especially below 1000 m/z. When MALDI is combined with ion mobility, its application widens and a variety of analytes can be qualitatively and quantitatively analyzed. Analytes trendlines are usually displayed on the drift time vs m/z plots according to their charge states and class of molecules. Lack of a universal calibrant that can be used inter-instruments and inter-laboratories in ion mobility has been a lingering challenge. We used MALDI matrix cluster ions mobility trendline shifts to correctly predict the drift times of PEG and AIP upon changing TWIMS parameters i.e. wave velocity and wave heights. PEG was chosen for its intrinsic polydispersity characteristic while AIP was chosen as a suitable

biopolymer representative. We prove that this dependence of the trendline shift with changes in ion mobility parameters can be used as internal reference in MALDI ion mobility mass spectrometry experiments

3.2 MALDI Ionization

Matrix assisted laser desorption ionization (MALDI)[43] is among the most commonly used soft ionization techniques which was developed decades ago and it's broad application has been successfully demonstrated[44-47]. The technique involves co-crystallization of the sample with the matrix (Conventionally weak solid organic acids e.g. CHCA, DHB, SA and CHCA which exhibit a strong resonance ultraviolet absorbing capability at the laser wavelength used), whose role is to strongly absorb the laser UV energy and ionize the sample through either donation of proton or accepting of proton from the analyte in positive and negative ionization modes respectively. A pulsed laser is used to generate the ions. Generation of ions in pulsed mode has made it compatible with time-of-flight (TOF) mass analyzer. (Figure 3.

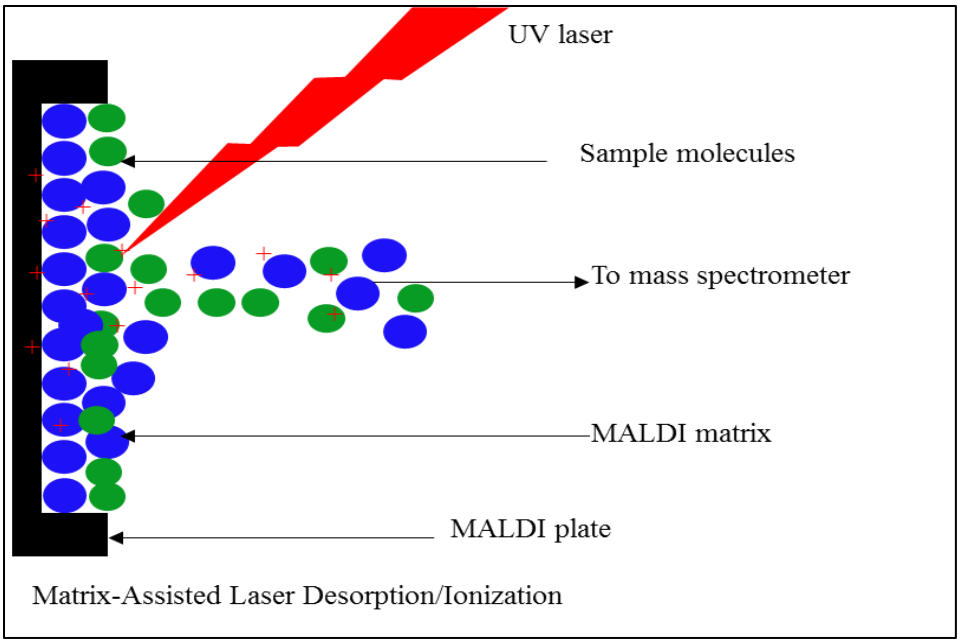

Figure 3.1. MALDI Ionization Process

Due to its advantages of requiring relatively low sample for analysis, higher sensitivity, high sample throughput, high tolerance of salts, rapid analysis and non-complex sample preparation process MALDI has become a great technique and has been applied in different type of samples analysis. Additionally, MALDI has an advantage of producing predominantly singly charged parent ions making it a suitable technique for analyzing a wide range of complex samples such as those found in metabolomics[48] and proteomics.[49] Although detailed mechanism of how analyte ions are generated in MALDI still remains controversial, there are models that propose the analyte ionization process.

They include; photochemical ionization[50] which suggests that collision of analyte molecules with matrix ions in the gas phase brings about protonation or deprotonation of the analyte. The other one is the cluster ionization[51] which proposes that strong UV

absorption by the matrix molecules causes ionization of the analyte upon desorption Chen et.al.[44] lately proposed energy transfer induced disproportionation mechanism where pseudo proton transfer happens during the co-crystallization of the matrix and analyte.

3.3. MALDI Matrix Cluster Ions

Accumulation of excitation energy in the matrix induces emission of explosive cluster which leads to formation of numerous intense cluster ions. These cluster ions are usually associated with the complication of analyzing analyte ions in the low m/z region ~1000 Da due to their interference with the analyte ions[52]. This interference affects the spectral quality and data interpretation thus increasing the detection limits compared to other ionization techniques like ESI. Since MALDI matrix cluster peaks which depends on the type of analyte, strength of the laser and amount of salt and metal adducts present are not reproducible and their appearance and relative intensities not predictable, the phenomenon makes some researchers shy away from using MALDI especially when the analytes fall in the low m/z region. However, there are various methods reported to expand the use of MALDI-MS in analyzing low mass range analytes and are discussed in detail here[52-54]

3.4 MALDI Ion Mobility

Due to the ability of generating ions in pulses, MALDI ionization source coupled with ion mobility mass spectrometry technique has seen its application broaden. Researchers have been able to directly profile and image tissues to elucidate structures of various analytes and map their distribution.[55] The incorporation of time-of-flight mass analyzers into commercially available instruments has facilitated this growth in

application.[56] Mass-mobility correlation lines hereby referred to as Trendlines are known to form according to both the class of molecular structures of the analytes and the charge states of the analytes.[36] These trendlines have been observed regardless of the instrument used in the analysis and both in the ESI or MALDI experiments. Since in MALDI, the dominant ions generated are usually singly charged the trend lines are easy to locate on the 2 D plot.

The focus of this research project is to explore the use of MALDI matrix cluster ions trendlines that are intrinsically generated during the matrix-assisted laser desorption/ionization (MALDI) ionization process as internal references for measuring the drift time in IM-MS analysis.

3.5 Experimental

3.5.1 Materials and Methods

3.5.1.1 Preparation of MALDI Matrices

When choosing a MALDI matrix, it is common practice to have a matrix whose laser wavelength absorption is high enough to facilitate ionization of the sample being investigated. Among other characteristics that must be met for a MALDI matrix to result in a successful MALDI experiment includes miscibility[1] with the analyte and solubility in the solvent of choice. For this study we investigated four widely used MALDI matrices chosen as representatives for all matrices i.e. CHCA, 3-HPA, DHB and SA. MALDI matrices that were used in this study were prepared using standard procedures that are available in literature. CHCA was prepared by dissolving 20.0 mg of CHCA in 1.0 mL of

50% ACN with 0.1% TFA and was stored away from light. 3-HPA was prepared by dissolving 35.0 mg of 3-HPA and 8.8 mg of ammonium citrate dibasic in 1.0 mL of 10 % CAN with 0.1% TFA and filtered as above. 2,5 DHB was prepared by dissolving 30 mg DHB in 30% acetonitrile and 0.1% trifluoro acetic acid. (Krause et al. 1999). Sinapinic acid (SA) was prepared by dissolving 20 mg of SA in 50% acetonitrile and 0.1% trifluoro acetic acid. The matrix solutions were vortexed for 1-2 minutes, filtered using 0.22-micron Non-sterile low protein binding Durapole (PDF) syringe driven filter membrane for fine particle removal and stored at −20 °C

3.5.2 Spotting

In each experiment, the matrix was mixed with equal volumes of the sample solution and a volume of ~0.2 µL pipetted on the wells of the dried droplet method used to dry the matrix and samples

3.5.3 Model Molecules

For prove of concept, two model molecules, Auto Inducing peptide (AIP), of molecular formula $C_{43}H_{59}N_8O_{13}S_2$ and monoisotopic mass 960.3721 Da to represent biomolecules. Figure. 3.2.a (Auto inducing peptide (AIP) standard C43H59N8O13S2=960.3721 Da) and Figure 3.2.b (Polyethylene glycol (PEG 1000)) were used.

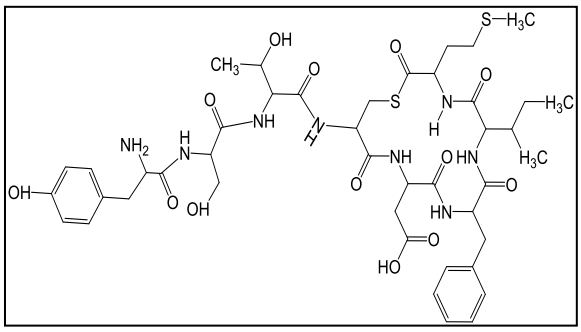

Figure 3.2.a. AIP Standard

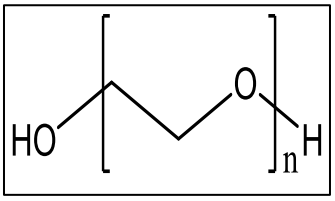

Figure 3.2.b. PEG 1000

3.5.4 Sample Preparation

Since MALDI as an ionization technique is widely used in both biomolecules and synthetic polymers, the molecular probe ions used in this study were selected with that fact in mind. The first model molecule, AIP-I, (Auto inducing peptide) (≥95% purity by HPLC) was obtained from AnaSpec Inc. (Fremont, CA) as a powder and was dissolved in 50:50 v/v acetonitrile: water to make 100 uM stock solutions and then diluted to 1 uM using 50 % acetonitrile with 0.1% TFA.

PEG (Polyethylene glycol 1000, Bioultra) was bought from Sigma Aldrich (Louis, MO) and was prepared by mixing 10 µL of PEG 1,000 with 2 mg/ mL of sodium iodide in 50 % ACN as outlined for calibration of the Waters Synapt G2 instrument by the manufacturer.

All the data was acquired using a hybrid Q-TWIMS-time-of-flight (TOF) MS (Synapt G2 High Definition Mass Spectrometer; Waters, Milford, MA, USA) equipped with interchangeable MALDI and ESI sources. The instrument operates in two modes i.e. T-Mode (TOF mode) where it separates ions according to their mass to charge ratio and

in M-Mode (Mobility TOF mode) where it separates ions according to size, shape and charge in addition to mass to charge ratio. The TOF analyzer in this instrument can be operated in three modes i.e. Sensitivity mode, where the ions travel in the TOF analyzer through a 'V' optics settings, Resolution mode which also have the ions travel through a 'V' optics settings and High-Resolution mode where the ions transit through a 'W' optics settings. The data reported here was collected in the resolution mode. The instrument was operated in the ion mobility mode with most parameter settings at the default i.e. Gas flow; Trap gas flow of 2.0 mL/Hr., helium gas flow at 180 mL/min and nitrogen gas at 90 mL/min. The HM resolution (sets the width of the quad transmission) was set at 4.4 as recommended by the manufacturer for MALDI experiments. For this study the wave velocity and wave height whose change affects the transit of ions according to the need of the experiment.

3.6 Results and Discussions

3.6.1 Spectrum Acquisition

3.6.1.1 MALDI Matrices

For prove of concept, all the MALDI matrices data was acquired both in positive (figure 1 a-d) and negative polarities at a consistent scan time of 1.0 second and acquisition time of 0.5 minutes for each experiment. The mass range was set at between 50 to 1000 m/z. The laser was set at an energy of 350 nm and data was acquired by manually moving the laser across the selected spot on the target MALDI plate to maximize ablation of the sweet spots with the laser beam on the unevenly spread co-crystalized sample and matrix mixture. All the MALDI matrices displayed mobility

trendline which shifted similarly with changes in ion mobility parameters. CHCA matrix was randomly chosen as a representative matrix for the studies that follow, in addition, positive polarity was employed in all data reported here. To reduce the noise on the mobility trendline and to easily detect sample and matrix cluster ions signals, the intensity threshold was reduced to between 30% minimum and 100% maximum using the driftscope software provided by Waters.

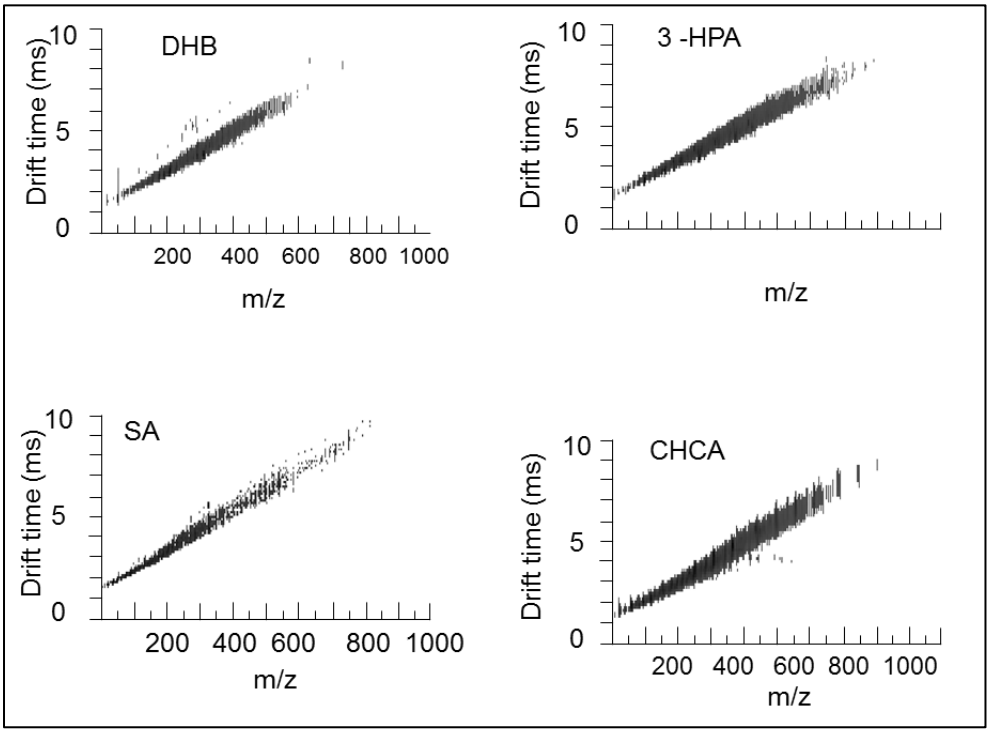

Figure 3.3.a to d. DriftScope Plots (Trendlines) of Different MALDI Matrices used in the Current Study.

Shift of the matrix cluster ions Mobility Trendline with change in parameter settings. To adjust the transit time of the ions in the traveling wave ion mobility cell, i.e. improve the separation of ions, there are two parameters amenable to adjustment i.e.

either the wave height or the wave velocity. To investigate the behavior of the trendline upon changing the parameters, wave velocity was changed from 650 m/s to 850 m/s and a shift of the trendline increasing the drift time of the matrix cluster ions thereof was observed (Figure 3.4. a. and b.)

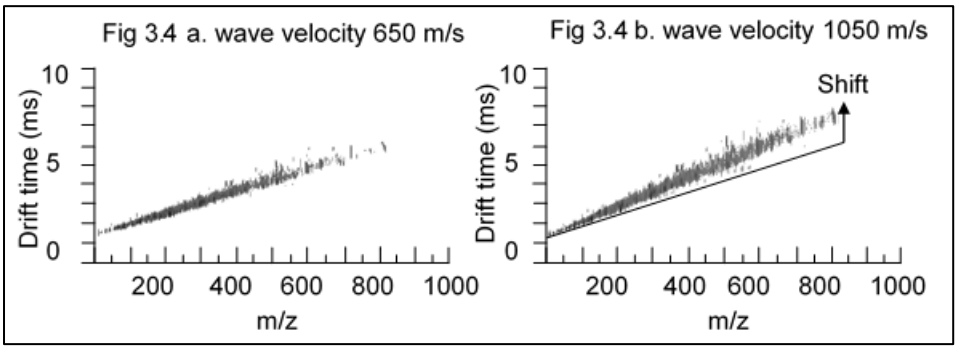

Figure.3.4. CHCA Matrix Trendline at Wave Velocities a. 650 m/s and b.1050 m/s

3.7 Linearity of the Mobility Trendline

To investigate the linearity of the trendline, drift times for selected MALDI matrix cluster ions mass peaks which showed consistency in intensity and accuracy across several experiments were acquired from their respective mobilograms and used to plot a reference curve. Automatic peak detection capability in the Driftscope software was used to transfer the drift times for these peaks to MassLynx, a software for analyzing mass spectrometry data. This enabled the selected peaks to be distinguished in the Driftscope, (a software which depicts mobility data in a 2 D plot with drift time vs m/z values and the intensity of the ions shown by varying shades of colors) figure 4.
Data was acquired by performing the experiment for each wave velocity three times

starting with the default; 650 m/s and then increasing to 850 m/s while keeping the wave height constant at the default setting 40 V.

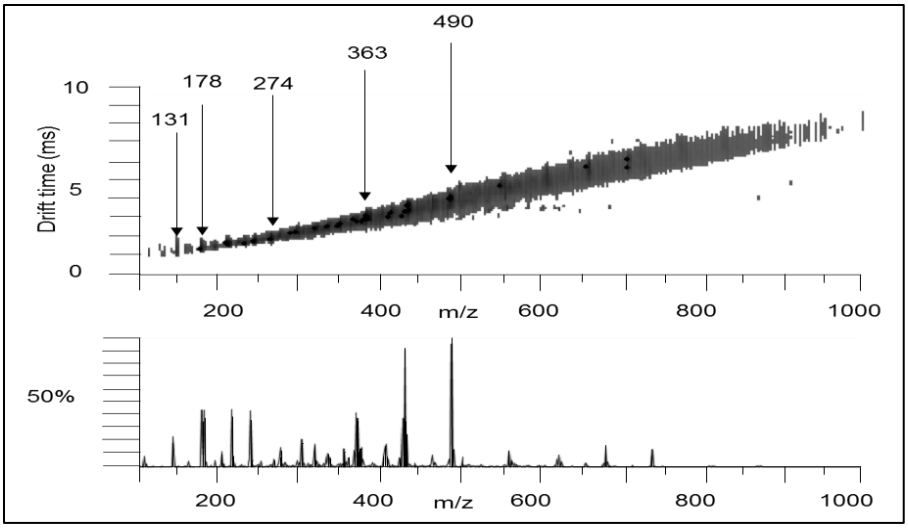

Figure 3.5. CHCA MALDI Matrix Cluster Ions Trendline with the Arrows Showing Selected Mass Peaks used for Generating the Reference Curve

A table of the m/z values of the selected matrix cluster ions mass peaks, average drift times at 650 m/s and 850 m/s and the standard deviation (Table 3.1) was used to plot a reference curve (for figure 5). The linearity of the curve was confirmed with the R^2 value, i.e. .9935

Table 3.1. Average Drift Times for Selected m/z Values Cluster Ions at Wave Velocities 650 m/s and 850 m/s

m/z	Av dt (850 m/s)	Average dt (650 m/s)	Av dt	SDEV
131.00	2.00	1.57	1.78	0.35
178.00	2.43	1.90	2.16	0.69
274.00	3.55	2.80	3.18	0.78
363.00	4.70	3.67	4.18	1.20
490.00	6.55	5.30	5.93	0.88

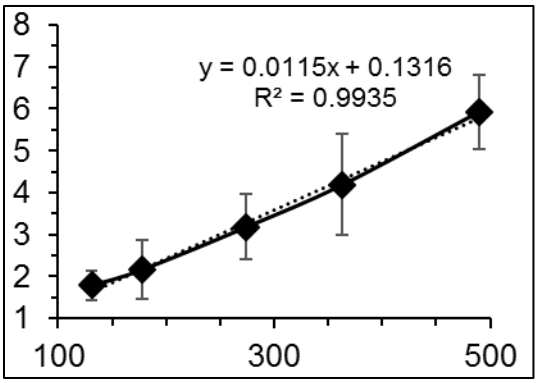

Figure 3.6. Average Drift Time for Selected m/z Values for CHCA Matrix Cluster Ions in Both Wave Velocities i.e. 650 m/s and 850 m/s

3.8 MALDI Matrix Co-crystalized with Model Molecules

After testing the effect of changing wave velocity on the shift of the matrix cluster ions trendline, Auto Inducing peptide (AIP) was co-crystalized with CHCA matrix to investigate the effect of the trendline shift on the drift time of the sample molecular ion.

To achieve this goal, both wave velocity and wave height were adjusted, and the drift time of AIP signal monitored.

3.9 Shift of the Trend Line with the AIP Signal

Conditions in the MALDI source, trap and transfer TWAVE cells were kept constant while the wave velocity and wave height in the ion mobility cell were changed systematically and the data acquired for each experiment. Since the goal was to investigate the drift time of the sample ion's signal with respect to the MALDI matrix cluster ions trendline, AIP was used since it displayed one discernable signal i.e. at the m/z value of 961 along the trendline after the front-end parameters of the instrument were optimized to minimize in-source fragmentation. The matrix cluster ions trendline shifted

together with the AIP signal with each change of the parameters. For instance, when the wave velocity was increased from the default settings i.e. 650 m/s to 850 m/s, the drift time for AIP changed from 8.6 ms (Figure 6 a.) to 11.3 ms (Figure 6 b) and, upon changing the wave heights from the default setting, 40 v (8.6 ms) Figure 6 c. the drift time changed significantly when the wave height was adjusted to 30 v (14.8 ms), Figure 6d.

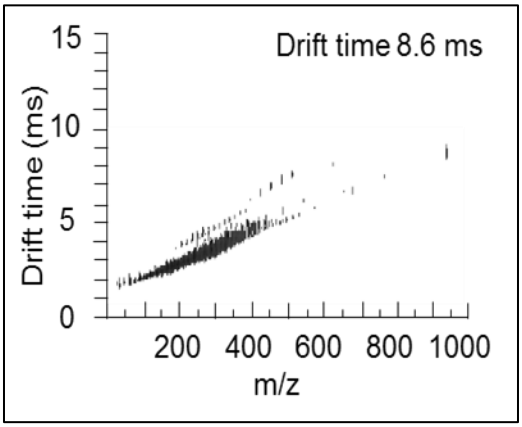

Figure 3.7.a. MALDI Matrix Ions Trendline for Wave Velocity 650 m/s

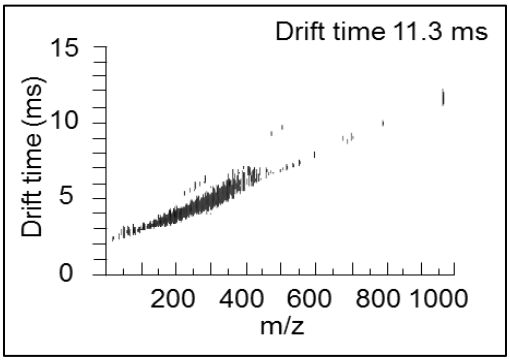

Figure 3.7.b. MALDI Matrix Ions Trendline for Wave Velocity 850 m/s

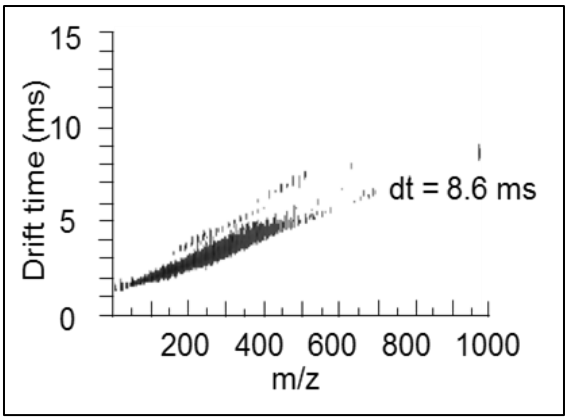

Figure 3.7.c. MALDI Matrix Ions Trendline for Wave Height 40 V

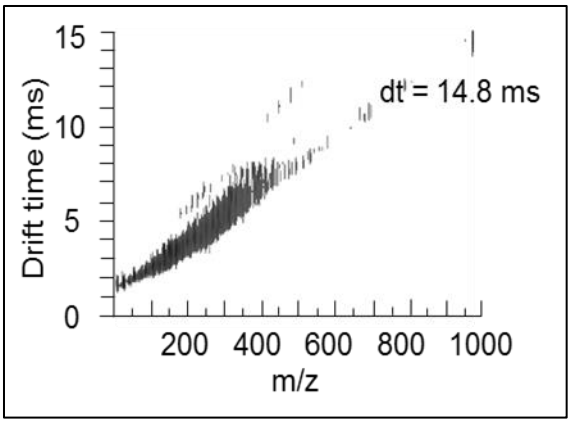

Figure 3.7.d. MALDI Matrix Ions Trendline for Wave Height 30 V

3.9.1 ESI IMS

A similar experiment was carried out in ESI mode with the AIP standard. With all other parameters remaining the same apart from the ionization mode and with optimization to decrease in-source fragmentation, the wave velocity and wave height were varied. The results indicate that the drift time of the AIP signal shifted in the same proportion as in MALDI (figure 3.8 a and b).

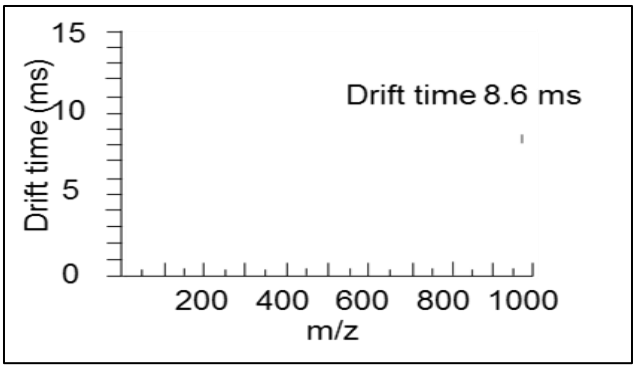

Figure 3.8.a. AIP Signal at Wave Velocity 650 m/s in ESI Mode

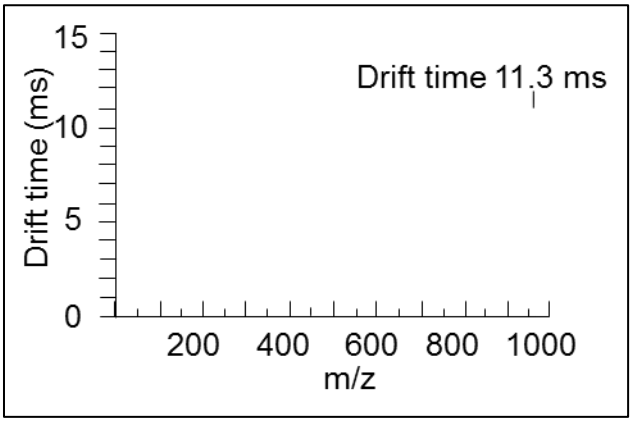

Figure 3.8.b. AIP Signal at Wave Velocity 650 m/s in ESI Mode

3.9.2 Internal Reference Curves

After observing that the shift of the trend line upon changing the wave velocity and wave heights happens with the sample ion signal, three different experiments using the same CHCA MALDI matrix stock solution at wave velocity 650 m/s and wave height 40 v were performed from the same target plate to get the respective drift times for the five selected MALDI matrix cluster ions mass peaks. The average drift times were used to plot a reference curve whose R^2 value was 0.9999 (Figure 3.9).

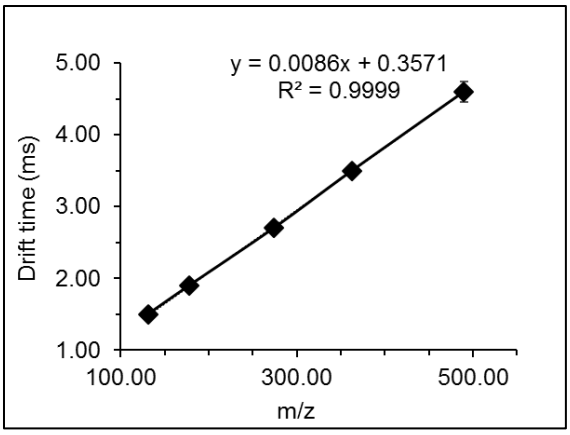

Figure 3.9. CHCA MALDI Matrix Cluster Ions Reference Curve from the Drift Time of the Selected Matrix Cluster Ions Mass Peaks at Default Settings.

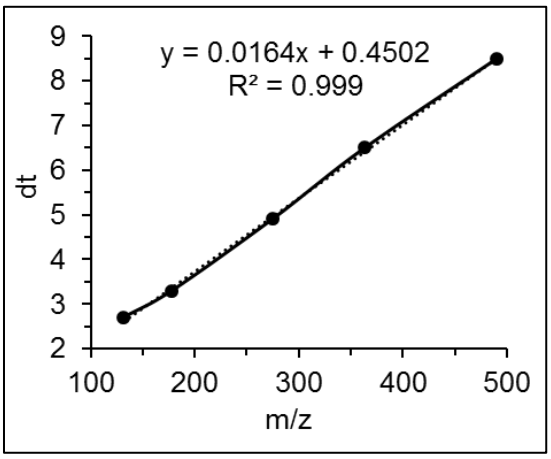

Figure 3.9.a. CHCA MALDI Matrix Cluster Ions Reference Curve Wave Velocity of 1250 m/s and Wave Height 40 V

3.9.3 Using Internal Reference Curve to Predict Drift Times for AIP

To characterize the applicability of the reference curve in predicting the drift times for sample molecular ions, experiments were repeated with MALDI matrix co-crystalized with the respective samples. For a start, the parameters were set at default settings i.e. wave velocity of 650 m/s and a wave height of 40 v. For AIP, upon acquiring

the mass spectrum for the sample/ matrix mixture, the drift times for the AIP were directly read from the m/z extracted mobilograms and the equation for the reference curve used to predict the drift time of the sample (calculated value). To establish the reproducibility of these approach, each analysis was repeated three times in different days and without changing the parameters, target plate, the sample or the matrix solution. The percentage error for all the trials were found to be >1.5 as shown in table 3.2

Table 3.2. Application of CHCA Matrix Cluster Ions Reference Curve on AIP Sample Wave Velocity 650 m/s and Wave Height 40 V

	Trial 1	Trial II	Trial III
AIP m/z	961.19	961.13	961.13
Calculated drift time (ms)	8.62	8.62	8.62
Measured drift time (ms)	8.60	8.50	8.50
% Error	0.23	1.41	1.41

Table 3.3. Application of CHCA Matrix Cluster Ions Reference Curve on AIP at Wave Velocity 850 m/s and Wave Height 40 V

	AIP drift time		
	Trial I	Trail II	Trail III
Calculated	11.27	11.21	11.32
Measured	11.25	11.25	11.30
% Error	-0.18	0.36	-0.18

Similar reference curves for different wave velocities i.e. 850 and 1250 m/s were tested and the percentage error for drift time prediction of the AIP was found to be 0.18% for wave velocities 650 m/s and 1250 m/s.

3.9.4 Using Internal Reference Curve to Predict Drift Times for a Polydisperse Sample

To validate our reference curve, a different molecular ion in structure from AIP was employed. PEG 1000 was chosen due to its intrinsic polydispersity thus the ability to offer numerous ions covering a broad mass range and a large m/z window to test the reproducibility of the reference curve. In addition, PEG 1000 ions are reported to maintain their conformations amidst instrumental conditions in an experiment using the same instrument.[40] Selected m/z values within the CHCA matrix cluster ions mass range and outside the matrix range were used to validate our results with AIP sample. Extraction of the drift times for the selected m/z ions was done as previously explained and the percentage error calculated. The average percentage error for all the ions was found to be 1.92 and all the ions had the percentage error < 4% (Table 3.5).

Table 3.4. Application of CHCA Reference Curve with PEG Sample, at Default Velocity 650 m/s and Height 40 V

PEG m/z	Calculated dt (ms)	Measured	% Error
349.18	3.36	3.20	-5.00
393.21	3.74	3.60	-3.85
437.24	4.12	4.10	-0.42
525.29	4.87	4.80	-1.55
614.34	5.64	5.40	-4.45
745.42	6.77	6.80	0.47
807.34	7.30	7.40	1.35
965.55	8.66	8.90	2.69
1229.71	10.93	11.50	4.93

3.9.5 Conclusion

The goal of this study was to use the intrinsic co-crystalized matrix ions as internal reference in ion mobility. Based on the comparison between calculated and measured drift times using the reference curves obtained from selected matrix cluster ions drift times, we have demonstrated that intrinsic MALDI matrix cluster ions can be applied in predicting with relatively high accuracy the respective analyte ions drift times regardless of the parameter changes. Indeed, the percentage error for both molecular model ions used in this study was found to be > 5%. For the proof of concept, travelling wave ion mobility instrument, Synapt G2 is used. However, the approach of using internal reference to improve the accuracy of IM-MS measurements can be applicable to other MALDI ion mobility mass spectrometry platforms.

CHAPTER IV

EFFECTS OF DIFFERENT MODES OF OPERATIONS ON TOTAL INTERNAL ENERGY OF IONS IN TWIMS

4.1 Introduction

The demands for achieving higher accuracy to detect known or unknown analyte has and will always continue in many areas of scientific research. The same has occurred on improving the resolution of traveling wave ion mobility mass spectrometry to distinguish isobaric ions with very close collisional cross sections. This led to a successful launch of the second generation of a commercialized technology on traveling wave ion mobility spectroscopy. Besides the performance on resolving collisional cross section, the principle of traveling wave ion mobility as well as the unique instrumental design in the Waters Synapt G2 have drawn research interests to study the additional outcome from carrying out the ion mobility measurements. In this study, the use of a simple experimental approach to estimate the variation on the total internal energy of ions as a result of changing the setting of a specific parameter is demonstrated.

The approach is based on carrying out a series of MS/MS experiments by sequentially increase the collision energy in the transfer cell after the ion mobility separation is completed. Thus, neither modification in the instrumentation nor any theoretical calculation for the ion energy is required. The results of using this approach do comply with the earlier reports on studying the effects of the same parameters. Based on the estimation by using this approach, the variation of ion energy could be more than 10eV. The information on the variation of ion energy as a result of using different parameter settings can potentially be useful for setting up and/or interpreting the results of MS/MS experiments as well as avoiding any unwanted conformational change of larger molecular ions or ion dissociation when target ions are analyzed by using traveling wave ion mobility mass spectrometry

4.1.1 Ion Mobility Mass Spectrometry

The coupling of ion mobility spectrometry to mass spectrometry is considered as a game changer for molecular analysis. The ion mobility spectrometry can provide information on the mobility of ions in the gas phase, which depends on the mass, charge and shape of ions. By combining with the information available from carrying out mass spectrometric measurements, it certainly helps to improve the accuracy on analyzing a variety of sample types[17, 18]. With the ability to distinguish ions with different shapes, the ion mobility spectrometry can be very useful for analyzing structural isomers, which could be co-eluted from a liquid chromatographic column and carry exactly the same molecular mass. Thus, the analysis of many isomers remains a challenge to the current approach of using liquid chromatograph mass spectrometry.

The ion mobility technology that has been successfully coupled to mass spectrometry include: drift tube[27, 28, 37] , differential ion mobility or high-field asymmetric waveform ion mobility[57], traveling wave[30] and trapped ion mobility[58]. Among the commercialized platforms for ion mobility mass spectrometry (IM-MS), the Waters Synapt series which base on the traveling wave technology has a unique and most versatile instrumental design[32-34]. In the Waters Synapt IM-MS instrument, following a switchable ion source, the ions can be sorted out by a quadrupole mass filter before reaching to the setup for traveling wave ion mobility separation. To the best of our knowledge, the Waters Synapt is the only commercialized IM-MS platform that offers the ability to select specific molecular ions prior to the ion mobility separation. After the ions are transmitted across the traveling wave ion mobility cell, the accurate mass of ions is measured by an orthogonal time-of-flight mass analyzer. Within the setup for traveling wave ion mobility separation, it first starts with a trap cell whose primary function is to convert the continuous flow of ions from the quadrupole into batches of ions. Each batch of ions is then analyzed in the traveling wave ion mobility cell. Since the traveling wave operates under a higher gas pressure than the subsequent time-of-flight mass analyzer, there is a transfer cell at the end of the setup. The unique design of Water Synapt includes making both trap cell and transfer cell to be available for the dissociation of ions. In other words, there are two consecutive collisional induced dissociation (CID) cells, one before the ion mobility cell and one after the ion mobility cell.

The drawback of the current ion mobility technology including the traveling wave technology are the lack of high resolving power to distinguish larger ions with similar

collisional cross sections and the poor yield of ion transmission. In the latter case, one of the possible contributing factors could be the heating of ions inside the ion mobility cell, which may lead to unintended ion dissociation. To address this issue for using the Waters Synapt IM-MS platform, several research groups have attempted to determine the thermal status of ions inside the ion mobility cell. For instance, De Pauw et.al. reported the use of p-methoxybenzylpyridinium as a thermometer ion to determine the vibrational effective temperature of ions.[59] Whereas, Merenbloom et.al. reported using the dissociation of protonated leucine enkephalin dimer as a probe and theoretically calculate the effective temperature of ions in the ion mobility cell.[60] Shvartsburg and Smith used the mobility of ions to estimate the range of temperature rise in the ion mobility cell.[33] In this report, the use of a simple approach to estimate the variation on the total internal energy of ions is explored, which may result from using different settings of the key parameters in the traveling wave ion mobility mass spectrometry.

4.2 Materials and Methods

4.2.1 TWIMS Parameter Settings

All experimental data was acquired using a Waters Synapt G2 high definition mass spectrometer (Waters, Milford, MA, USA) equipped with an ESI source. The instrument was calibrated with Leucine enkephalin for mass accuracy and polyalanine for ion mobility accuracy as recommended by the manufacturer. The sample was delivered by direct infusion at a flowrate of 10 μL/min. The instrument was operated under the mobility TOF mode. The source temperature was set 120^{o}C, the desolvation temperature at 240^{o}C, the cone gas flowrate was maintained at 50L/hr., and the desolvation gas

flowrate at 50L/hr. while the other ESI parameters were optimized for an effective ion transmission. Unless otherwise stated, the traveling wave ion mobility cell was operated under the default settings, which included a flow of Argon gas to the Trap and Transfer cell at 2mL/min, a flow of Helium gas to the Helium cell at 180mL/min, a flow of Nitrogen gas to the ion mobility cell at 90mL/min, wave height at 40V, and wave velocity at 650m/s). To minimize the fragmentation of ions in the ion mobility cell, IMS bias voltage was set at 3V. The TOF mass analyzer was operated under the resolution mode, and the negative ion mode was used. In each experiment, the signals obtained from the sample was acquired for 1 minute and at a scan time of 1 second.

4.2.2 Adenosine 3′-Monophosphate (AMP)

The AMP ion at 346m/z was selected as the precursor ion. AMP was purchased as lyophilized powder with 99% purity (Sigma Aldrich, St. Louis, MO, USA) and was used without any further purification. A stock solution of 1 g/L was prepared by dissolving AMP in autoclaved deionized water and stored at -20^{0}C. Before the experiments, 10µM AMP was freshly prepared from the stock solution by using 50:50 H_2O: MeOH as a diluent. For calculating the % dissociation of AMP precursor ion, the fragment ions of PO_3^- at 79m/z, adenine at 134 m/z, and pentose phosphate at 211m/z were selected. The MS/MS spectrum of AMP was retrieved by integrating 1min time in the ion chromatogram. The ion counts for the precursor ion and the selected fragment ions were used to calculate the percentage of dissociation using the equation below.

$$\%\ \text{dissociation} = \frac{F}{P+F} \qquad \text{equation 1}$$

Where F is the sum of ion counts of selected fragment ions, and P is the ion count of remaining precursor ion (if any).

4.3 Results and Discussion

4.3.1 Using Different Wave Heights

According to the instructions from Waters on using the Synapt G2 to differentiate isobaric ions with different molecular shapes, the key parameters for optimal separation of isobaric ions are the wave height and/or wave velocity in the traveling wave ion mobility cell. De Pauw and his associates had reported the vibrational effective temperature of ions in traveling wave ion mobility mass spectrometry was increased as a result of increasing wave height[59]. In this report, by allowing a specific precursor ion passing through the ion mobility cell in the mobility TOF mode and sequentially increase the collision energy in the Transfer cell, the extent of ion dissociation (% dissociation), which is the result of a typical MS/MS experiment, starts from barely detectable level to increase proportionally with the increasing collision energy being applied to the Transfer cell, and eventually levels off at 100% dissociation when excessive collision energy is used (Figure 4.1).

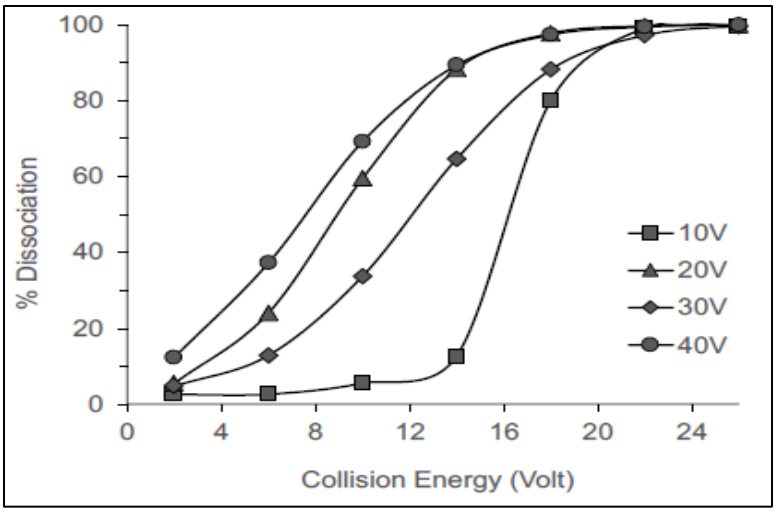

Figure 4.1. Effects of Varying the Setting of Wave Height in Voltage (V) in the Traveling Wave Ion Mobility Cell of Waters Synapt G2

While the parameter settings remain unchanged except the wave height is decreased from the default setting at 40V, the % dissociation curve of the same precursor ion starts to shift towards the right-hand side in Figure 1, i.e. higher collision energy. This result does comply with the principle of ions surfing along the traveling voltage wave, thus experience the changes in the wave voltage.[31] To ensure the positioning of the % dissociation curves in Figure 1 is reproducible, the same MS/MS measurements were repeated four times, and the coefficient of variation of % dissociation was calculated. The average coefficient of variation among the data points in a % dissociation curve was as low as 1.7%. Hence, the error bar of each data point is too small to be effectively shown in Figure 1. With the Transfer cell located right next to the exit of the ion mobility cell, the requirement for using higher collision energy in the Transfer cell to achieve the same level of ion dissociation represents the total internal energy of ions was lowered as a result of decreasing the wave height from 40V. In other words, there is a direct

proportional relationship between the total internal energy of ions and wave height. In this study, the total internal energy of ions is defined as the sum of all the rotational, vibrational, kinetic and potential energy of the ions.

Without making any changes in the instrumentation or applying any new theoretical calculations for the energy of ions, the results of using this rather simple approach to evaluate the ion energy do agree with De Pauw's finding on the direct proportional relationship between vibrational effective temperature of ions and wave height. In comparison to a report from Williams, in which the effective temperature of ions was measured, the approach in this study uses a precursor ion that is more thermally stable, thus the ion dissociation does not occur until the ions reach the Transfer cell.[60] Also, the complete dissociation curve is acquired and compared with another dissociation curve. As indicated above, no additional drift time measurement is required to estimate the variation on the total internal energy of ions.

Based on the same concept on interpreting the results in Figure 1, the extents of variation on the total internal energy of ions that result from changing the wave height can be estimated. The process begins with deriving the equations to calculate the required collision energy to achieve a specific level of ion dissociation. By isolating the linear portion of a % dissociation curve in Figure 4.1 and perform a linear regression analysis, the corresponding equation is derived. After working out all the required collision energies to achieve the same level of ion dissociation with different wave heights, the differences in the required collision energies are good approximation for the changes in the total internal energy of ions. This is due to the facts that the ion of interest has only

one single electrical charge, and the ion collision in the Transfer cell is the result of adjusting the Transfer collision energy, which is the voltage being applied to the entrance of the Transfer cell. This, in turn, changes the potential difference between the exit of the ion mobility cell and the entrance of the Transfer cell. When the ions exit from the ion mobility cell, the electrical energy is applied to the ions, which is then converted into the kinetic energy of the ions. While the pressure of Argon gas inside the Transfer cell remains constant, the ions collide with the Argon gas and the ion fragmentation occurs.

Thus, the difference in the required collision energies to achieve the same level of ion dissociation under two different settings of wave height is a good approximation for the variation on the total internal energy of ions which results from changing the wave height. For example, at the level of 50% ion dissociation, changing the wave height from 40V to 10V, the total internal energy of the selected precursor ion was calculated to be 9.0eV lower. The other variations in the total internal energy of ions from changing the wave height are shown in Table 1. This information is applicable for setting up and/or interpreting the results of MS/MS experiments in the mobility TOF mode. In contrast, this information can also be useful to avoid some unwanted conformational change of larger molecular ions or ion fragmentation in the mobility TOF mode by simply lowering the wave height accordingly.

Table 4.1. Extent of Variation of Total Internal Energy of Ions Resulted from Changing the Wave Heights Between 10 V and 40 V

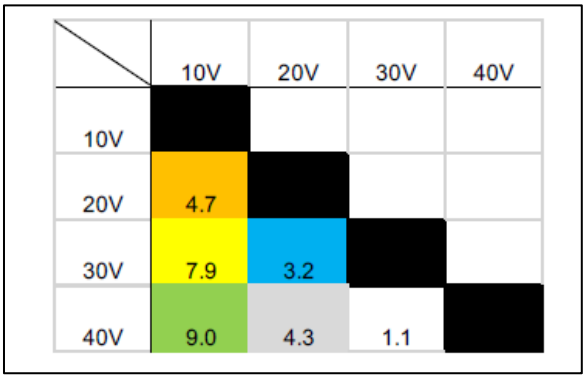

4.3.2 Using Different Wave Velocities

In studying the effects of wave velocity on the total internal energy of ions, the wave velocity in the ion mobility cell was either increased or decreased from the default setting of 650m/s while all the other parameter settings remained constant including the wave height. The range of wave velocity from 250m/s to 1050m/s was evaluated. The results are shown in Figure 2A. When the wave velocity was decreased step-by-step from 1050m/s, the % dissociation curve of the same precursor ion was shifted towards higher collision energy, which means more collision energy was required in the Transfer cell to achieve the same level of ion dissociation. This, in turn, represents the use of slower wave velocity leads to lower total internal energy in the precursor ions. In other words, there is a direct proportional relationship between the total internal energy of ions and wave velocity.

Since the total internal energy of ions should be directly related to the temperature of ions including its vibrational effective temperature, which as mentioned above was

investigated by De Pauw and his associates. According to De Pauw's finding, there is an inverse proportional relationship between the vibrational effective temperature of ions and wave velocity, i.e. the opposite to what have been observed in this study (Figure 4.2.).[59]

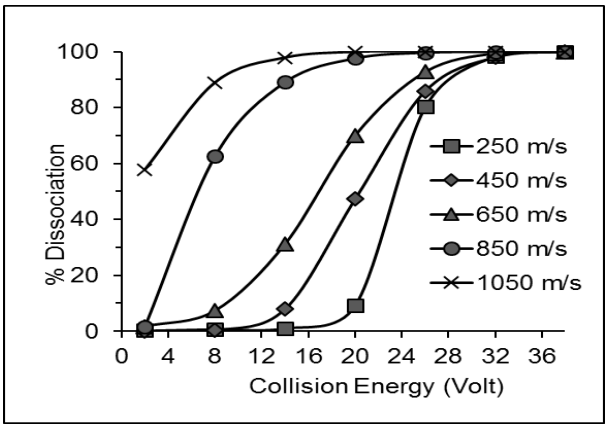

Figure 4.2. AMP Ions % Dissociation Against Transfer Cell Collision Energy at Different Wave Velocities

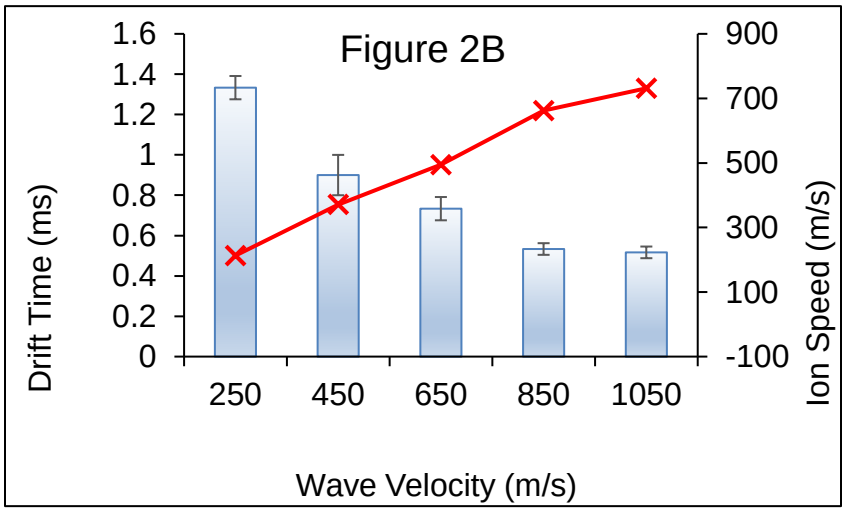

Figure 4.3. Bar Chart Representing the Variation of Drift Time in Milliseconds (ms) of the Precursor AMP Ions at Different Wave Velocities

To further investigate the relationship between the total internal energy of ions and wave velocity, the drift time of the selected precursor ion was measured at different wave velocities. The results are shown in Figure 2B. The lower the wave velocity, the longer the drift time was measured. These results do comply with the principle of ions surfing on the traveling voltage wave that exists inside in the ion mobility cell. If the wave travels at a slower velocity, it would take a longer time for ions to travel across the ion mobility cell, i.e. longer drift time. Based on the measured drift time, and approximating the length of the ion mobility cell to be 0.185 meter, the ion speed of the precursor ions while traveling across the ion mobility cell with different wave velocities were calculated by using the equation derived by Shvartsburg and Smith as shown below.[13]

$$v^2 = 2\, v_{d(TW)}\, s^2 / (s + v_{d(TW)}) \qquad \text{equation 2}$$

Where v is the ion speed, s is the wave velocity, $v_{d(TW)}$ is the drift velocity which is equal to the length of drift cell divide by the drift time of selected ion. In Figure 2B, the results of this study show the calculated ion speed increases with increasing wave velocity. As De Pauw and his associates had pointed out, the ion speed is a good predictor of ion effective temperature.[15] If ion speed goes up with increasing wave velocity as reported by De Pauw, the ion effective temperature should also go up, which in turn increases the total internal energy of ion. Hence, the direct proportional relationship between the total internal energy of ions and wave velocity in Figure 2A is

confirmed. In summary, the results from using the approach of % dissociation curve to evaluate the ion energy do agree with the other finding reported by De Pauw.[15]

4.4 Absence of Buffer Gas

In view of the variation on the total internal energy of ions from varying the wave height or wave velocity in the ion mobility cell, the extent of ion heating in the traveling wave was investigated by using the same approach of % dissociation curve. In this study, the % dissociation curve acquired by using the default settings was considered as a reference (Figure 4.3).

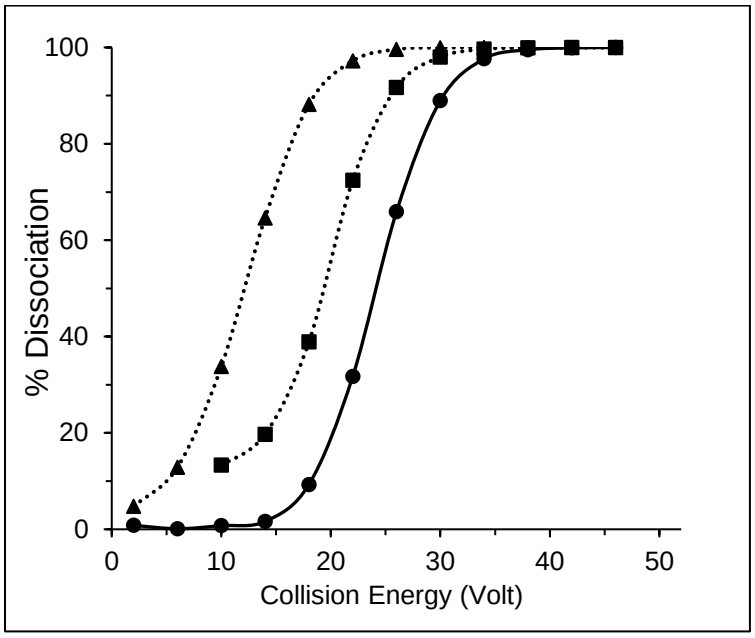

Figure 4.4. Extent of Ion Heating Without one of the Buffer Gases in the Traveling Wave Ion Mobility Cell of Synapt G2

By using the same precursor ion and without changing any parameter settings except turning off the supply of either one of the two buffer gases.

(Helium or Nitrogen) in the ion mobility cell, two additional % dissociation curves were acquired, which corresponded to either Helium off or Nitrogen off in Figure 3. In the absence of one of the buffer gas in the ion mobility cell, the % dissociation curves are shifted to the left-hand side of the default curve which corresponds to the presence of both buffer gases. Shifting the % dissociation curve to the left means lower collision energy was required to achieve the same level of % dissociation. This, in turn, represents the total internal energy of precursor ion was increased when one of the buffer gases in the ion mobility cell was absent. This result does comply with the ion heating reported before when traveling wave ion mobility mass spectrometry was used.[16,17] Thus, the approach of using the % dissociation curve to estimate the variation on the total internal energy of ion is validated and its applicability is demonstrated in this report. The bigger increase in the total internal energy of ions with the absence of Nitrogen buffer gas indicates more ion heating occur in the ion mobility cell than in the Helium cell or in the absence of Helium gas. Based on the shifting of the % dissociation curves in Figure 3, the extent of ion heating as a result of transmitting the ions across the ion mobility cell was estimated to be ~11.5 eV.

4.5 Conclusion

By making use of the unique and versatile design in the Waters Synapt G2 instrument, this report demonstrates the feasibility of using a simple yet applicable approach to estimate the variation on the total internal energy of ions which results from using different settings of the key parameters in the traveling wave ion mobility mass spectrometry. There are pros and cons on the results of ion heating when ions are exposed

to the traveling wave within the ion mobility cell. If ion dissociation is desirable after the ion mobility separation, the ion heating will be helpful. On the other hand, for the analysis of larger isobaric ions, the ion heating may lead to conformational changes, which will lead to incorrect drift time measurements and sample identification. To control the ion heating in the traveling wave ion mobility cell, different parameter settings in the ion mobility cell can be used. The developed approach can provide a simple way to estimate the extent of changes in ion energy which result from using different parameter settings in traveling wave ion mobility mass spectrometry.

CHAPTER V

HIGH PERCENTAGE OF ISOMERIC HUMAN MICRORNAS AND THEIR ANALYTICAL CHALLENGES

Parts of the work presented in this chapter has been published in the journal of non-coding RNA as referred as Joseph N. Mwangi, and Norman H. L. Chiu, Non- coding RNA 2016, 2(4),13

4.1 Introduction

In comparison to the structures of other biopolymers that exist in the living cells, ribonucleic acid (RNA) has a smaller set of monomeric units, which consist of four ribonucleotides, namely adenosine (A), uridine (U), guanosine (G), and cytidine (C). Furthermore, two of the nucleobases are purine and the other two are pyrimidine. Despite of this rather simple RNA structure, the biological functions of RNA have continued to grow. In order to create the complex RNA functions, single-stranded RNA molecules rely on the Watson-Crick base pairing and the intramolecular interactions with the hydroxyl group at the 2' position of each ribonucleotide to generate relatively stable RNA folding. To overcome the limitation on having only four canonical ribonucleotides, RNA may undergo over 100 different types of RNA modifications, which in turn may induce unique RNA structures and/or functions[65-72]. In general, RNA are categorized by their functions. For example, messenger RNA are templates for protein synthesis, whereas transfer RNA

convert the genetic codes [73]into their corresponding amino acid residues during the protein synthesis. Since the discovery of small non-coding microRNA (miR), more than 2,000 human miR have been identified[74-77]. Specific miR can post-transcriptionally regulate gene expression by binding directly with a messenger RNA, which results in either blocking the biosynthesis of corresponding protein or cleaving the messenger RNA with the assistance from a protein called Dicer[78-81]. In both cases, the binding between a specific miR and its messenger RNA target does not require 100% complementary base matching. This binding mechanism, therefore, allows the same miR to regulate more than one specific gene expression.

Collectively, miR is estimated to regulate as much as ~60% of gene expression in our bodies. Many specific miR have been associated to various diseases. In some cases, several different miR are reported to be associated with the same disease[82-88]. Besides serving as diagnostic and/or prognosis biomarkers, some miR have also been recognized as potential drug targets[89-94]. To further explore the potentials of miR in medical related studies, accurate detection of a specific miR is critical. All the current analytical methods for miR detection rely on the ability to distinguish a particular RNA structure, which may include its size, nucleotide composition and/or RNA sequence[95]. Although the structural information on human miR have been available for some time, no study on comparing their structural similarity has been reported yet. In this report, we determine the extent of structural similarity among all the human miR; and discuss its consequence to the detection of miR.

5.2 Results and Discussion

5.2.1 Size Distribution of Human MicroRNA

In the literature, the reported values for the minimum and maximum size of mature human miR often vary. Besides the possible errors in the earlier reports, this discrepancy could also be due to the ever-expanding list of human miR. Based on the information that was available from miRBase on August 2016, an attempt to determine the correct minimum and maximum size of human miR was carried out in this study. There are in total 2,588 human miR. The size of the mature human miR ranges from 16 to 28 nucleotides (Figure 1.2).

This makes the average size of mature human miR to be 22 nucleotides. As shown in Figure 1.2, among all the human miR, 44% of them have the same size and equal to the average size of 22 nucleotides. Only 16% of mature human miR have the size of either smaller or equal to 20 nucleotides. The rest of the human miR are longer than 22 nucleotides. The size distribution of human miR explains why the probe-based methods, in which a complementary DNA oligo or an analogue is used as a molecule probe to recognize a specific miR analyte, is a viable approach for the detection of human miR. If an RNA molecule has 20 nucleotides, it theoretically creates 4^20 or over one trillion possibilities for its RNA sequence. In other words, the RNA sequence of each human miR is unique in the entire human transcriptome, thus the recognition of a specific miR by matching its RNA sequence with a complementary DNA probe should provide sufficient specificity. However, in practice, non-specific binding of DNA probe is often unavoidable, especially when the size and the annealing position of the DNA probe are

fixed by the actual size of miR. If non-specific binding is not eliminated, it will lead to false-positive results on the detection of miR. To address this issue, different ways to improve the specificity of probe-based methods have been reported[96, 97]. However, similar to many other analytical measurements, the outcome from using any specific method to detect miR will partly depend on the sample complexity. To the best of our knowledge, there is currently no specific method for isolating only miR from a biological sample. The closet purification method that is available for miR research can only remove RNA longer than 200 nucleotides from a total RNA sample[98, 99]. Hence, transfer RNA and other types of RNA smaller than 200 nucleotides may co-exist with human miR in the same sample. In order to achieve high specificity and accuracy on the detection of miR, the information on the similarity of the properties of human miR can be very useful. For this reason, the rest of this report focuses on comparing the nucleotide composition and RNA sequence of human miR.

5.3 Isomeric MicroRNA

If two different RNA molecules have the same size and identical nucleotide composition, they would be chemically defined as isomers. It is important to note that an acronym called isomiR has been reported in the literature, and it does not refer to isomeric miR[100]. Among all the mature human miR, 1,432 (or 55%) of them are isomeric. As shown in the figure below.

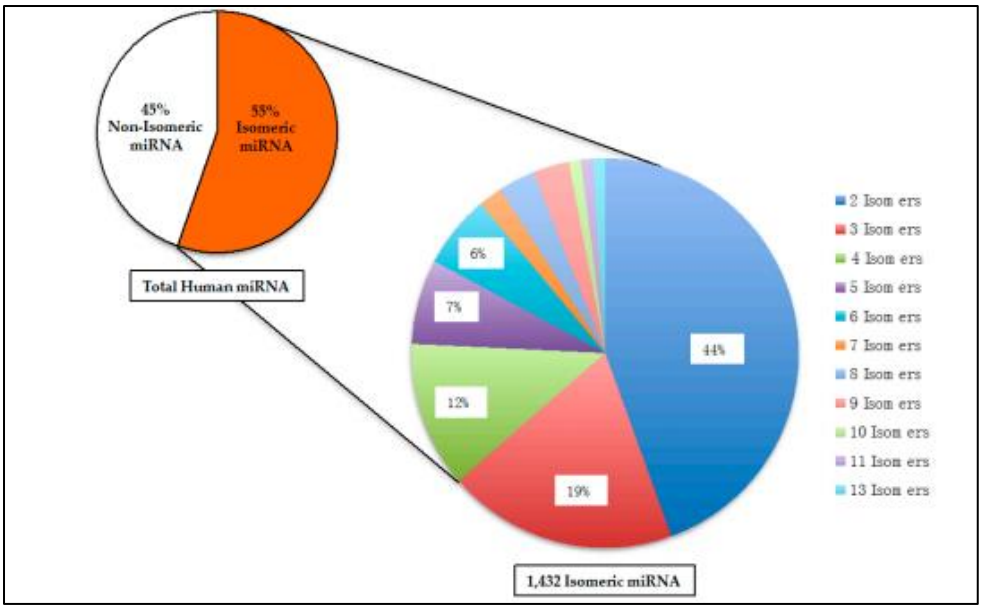

Figure 5.1. Distribution of Isomeric and Non-Isomeric Human Mature microRNA

Among the groups of isomeric miR, the highest number of isomers is 13, and there is only one group of 13 isomers. Majority of the human isomeric miR (44%) belong to the group of 2 isomers. In total, there are 315 different pairs of isomeric miR. Similar to the other types of RNA molecules, the modifications of miR have been reported, which include both adenylation and uridylation. The results of those RNA modifications would change the RNA sequence of miR, which may then alter the extent of miR isomerism. However, due to the lack of information on those RNA modifications in the entire collection of human miR, it is beyond the scope of this report to determine and compare the various extents of miR isomerism with or without any RNA modifications.

Table 5.1. The Largest Group of Structural Isomers Among all the Human microRNAs

miRNA	Sequence (5′–3′)	Chromosome	Location
miR-21-5p	UAGCUUAUCAGACUGAUGUUGA	17	NC_000017.11 (59841266..59841337)
miR-95-3p	UUCAACGGGUAUUUAUUGAGCA	4	NC_000004.12 (8005301..8005381)
miR-100-3p	CAAGCUUGUAUCUAUAGGUAUG	11	NC_000011.10 (122152229..122152308)
miR-513b-5p	UUCACAAGGAGGUGUCAUUUAU	X	NC_000023.11 (147199044..147199127)
miR-519a-3p	AAAGUGCAUCCUUUUAGAGUGU	19	NC_000019.10 (53752397..53752481)
miR-519b-3p	AAAGUGCAUCCUUUUAGAGGUU	19	NC_000019.10 (53695213..53695293)
miR-522-3p	AAAAUGGUUCCCUUUAGAGUGU	19	NC_000019.10 (53751211..53751297)
miR-548am-5p	AAAAGUAAUUGCGGUUUUUGCC	X	NC_000023.11 (16627012..16627085)
miR-548c-5p	AAAAGUAAUUGCGGUUUUUGCC	12	NC_000012.12 (64622509..64622605)
miR-548h-5p	AAAAGUAAUCGCGGUUUUUGUC	6	NC_000006.12 (131792172..131792231)
miR-548k	AAAAGUACUUGCGGAUUUUGCU	11	NC_000011.10 (70283955..70284070)
miR-548o-5p	AAAAGUAAUUGCGGUUUUUGCC	20	NC_000020.11 (38516563..38516632)
miR-4789-5p	GUAUACACCUGAUAUGUGUAUG	3	NC_000003.12 (175369540..175369621)

5.4 Disease-Associated Isomeric MicroRNA

Through many studies, a lot of human miR have been associated to diseases. In some cases, more than one specific miR is associated to the same disease. For this reason, whether the disease-associated miR would co-exist in the same biological sample or not, there are needs to measure as many disease-associated miR as possible. For instance, higher accuracy can be achieved by measuring a small panel of miR that are associated to the same disease. To evaluate the implication of miR isomerism to the detection of disease-associated miR, three different disease models were selected. The three selected disease models are colorectal cancer, malignant ovarian cancer, and epithelial ovarian cancer. Based on the information available from miR2disease database, the total number of disease-associated miR in each selected model is different from each other. In comparison to the entire collection of human miR, the distribution of isomeric miR in

each selected disease model is shown in Figure 3. In the case of colorectal cancer, there are 88 miR associated to the disease, and 67% of them are isomeric. In the case of malignant ovarian cancer, there are 78 miR associated to the disease and 65% of them can be isomeric to other human miR. In the case of epithelial ovarian cancer, there are 47 miR associated to the disease and 72% of them are isomeric. In comparison to the 55% of isomeric miR among all the human miR, the percentage of isomeric miR in the selected disease models are significantly higher

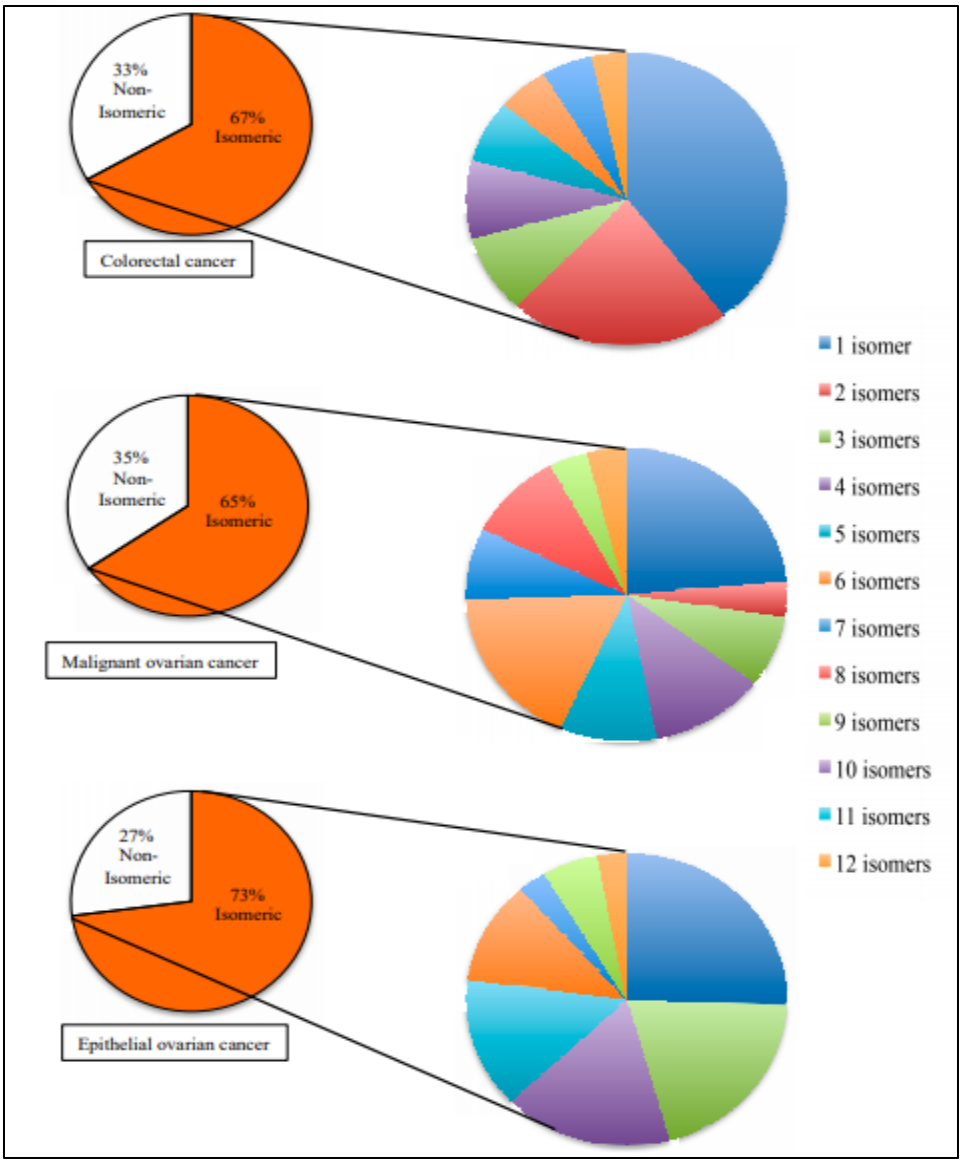

Figure 5.2. Extent of MicroRNA Isomerism Among Selected Diseases

The disease-associated microRNA are divided into three groups according to the diseases. The total number of disease-associated microRNA in each group is different - epithelial ovarian cancer has 47 microRNA, malignant ovarian cancer has 78 microRNA, and colorectal cancer has 88 microRNA. Within each group, microRNA are further

categorized by the number of isomers. The overlapping of the bar charts do not represent the same microRNA are associated to more than one of the selected diseases.

5.5 Sequence Similarities Among Isomeric MicroRNA

The minimum difference between the RNA sequence of two isomeric miR is one nucleotide. In Table 5.1, six different pairs of isomeric miR were found to be different by only two nucleotides. Although some of their names are very similar, the isomeric miR with high sequence similarity in Table 5.1 are encoded by different genes. With the high sequence similarities, these isomeric miR are expected to target the same messenger RNA. Hence, it is important to accurately determine which particular isomer is responsible for a specific post-transcriptional regulation of gene expression

Table 5.2. Examples of Isomeric Human MicroRNA That Have High Sequence Similarities, and their Gene Location Within the Human Genome

miRNA	Sequence (5′–3′)	Chromosome	Location
let-7a-2-3p	CUGUACAGCCUCCUAGCUUUCC	11	NC_000011.10 (122146522..12214659)
let-7e-3p	CUAUACGGCCUCCUAGCUUUCC	19	NC_000019.10 (51692786..51692864)
miR-301b-3p	CAGUGCAAUGAUAUUGUCAAAGC	22	NC_000022.11 (21652981..21653058)
miR-301a-3p	CAGUGCAAUAGUAUUGUCAAAGC	17	NC_000017.11 (59151136..59151221)
miR-378a-3p	ACUGGACUUGGAGUCAGAAGGC	5	NC_000005.10 (149732825..14973289)
miR-422a	ACUGGACUUAGGGUCAGAAGGC	15	NC_000015.10 (63870930..63871019)
miR-20b-5p	CAAAGUGCUCAUAGUGCAGGUAG	X	NC_000023.11 (134169809..13416987)
miR-17-5p	CAAAGUGCUUACAGUGCAGGUAG	13	NC_000013.11 (91350605..91350688)
miR-148a-3p	UCAGUGCACUACAGAACUUUGU	7	NC_000007.14 (25949919..25949986)
miR-148b-3p	UCAGUGCAUCACAGAACUUUGU	12	NC_000012.12 (54337216..54337314)

5.6 Analytical Challenges from Isomeric MicroRNA

As summarized in Table 5.2, the current analytical methods for detecting miR can be divided into three categories. In terms of their analytical performance, each category has its pros and cons for the detection of a specific miR

Table 5.3. Current Categories of Analytical Methods for Measuring microRNA
.

Analytical Method	Specificity for Detecting Specific microRNA	Sample Throughput	Costs	Differentiation of Isomeric microRNA
By Sequencing	★★★	Low to High	$$–$$$	Yes
By Mass Measurement	★★★	Medium	$$	Size- and Sequence-dependent
By Complementary Probe	★★ to ★★★	Low to High	$$	Sequence-dependent

Theoretically, the applications of these analytical methods to differentiate isomeric miR are feasible but the outcome may vary. Firstly, there is no doubt the current sequencing methods including the next generation sequencing technology can differentiate isomeric miR even with high sequence similarities. However, in comparison to the other analytical methods, the next generation sequencing technology has the highest cost on the consumable materials and the highest demand on data analysis. For those analytical methods whose end point measurement involves measuring the mass, the molecular mass of isomeric miR are exactly identical, thus mass spectrometry with high mass resolution will not be useful for the differentiation of isomeric miR. Recently Biba and his co-workers101 had completed an in-depth study on using different chromatographic methods to resolve small isomeric RNA molecules with high sequence similarities. Their experimental results indicated that there are high probabilities for small

isomeric RNA to be co-eluted from a chromatographic column. Hence, the coupling of liquid chromatography to mass spectrometry may not provide sufficient resolving power to differentiate isomeric miR. Since 100% sequence coverage is not always achievable in tandem mass spectrometry of RNA, plus the mass difference between uridine and cytidine has only 1 Da, it remains challenging to re-sequence RNA with ≥ 22 nucleotides by using tandem mass spectrometry. Hence, there is limitation on using mass spectrometric methods to accurately identify or differentiate isomeric miR in a single sample. By optimizing the annealing conditions, the probe-based methods should have the ability to distinguish two or limited number of isomeric miR, providing the differences in the RNA sequence of isomeric miR are not at or near the 5' or 3' terminals. Also, the size and the annealing position of the DNA probe or its analogue are fixed by the actual size of miR.

5.7. Materials and Methods

In this study, the RNA sequence of mature human miR and the location of its corresponding gene in the human genome were downloaded from the latest version of miRBase (miRBase 21) database (http://www.mirbase.org) on August 19th 2015. The online Mongo oligo mass calculator v2.06 was used to calculate the nucleotide composition of each miR. In-house Excel-based tools were used to determine the size of miR and identify isomeric human miR. For the analysis of sequence similarity, MAFFT, a multiple sequence alignment tool which was freely accessible online was employed to generate the data according to the guidelines for the program.

The three models of disease used in this study were randomly chosen based on the information available from the miR2Disease database, which is a collaboration between Indiana University School of Medicine and the Harbin Institute of Technology[102]. Before analyzing the disease-associated miR data as described above in this section, the information of each individual miR was crosschecked with information in the miRBase database.

5.8. Conclusion

Based on the results of this study, the size of mature human miR ranges from 16 to 28 nucleotides, which is slightly different from the earlier reports. Among 2,588 mature human miR, 44% have the same size with 22 nucleotides. Despite of this bias in their size distribution, and the limitation of only four canonical ribonucleotides, each specific miR still has its own unique RNA sequence among the other RNA molecules in the human transcriptome. However, for the first time, we report a high percentage (55%) of mature human miR are isomeric. MicroRNA that have the same size and identical nucleotide composition are defined as isomeric miR and hereby referred as "SimiR" which stands for structural isomers of microRNA. In reference to the whole collection of human miR, SimiR have been identified among miR that have been associated to a specific disease. Although each SimiR has a unique RNA sequence, some SimiR have relative high sequence similarities. Since all the current analytical methods for the detection of miR rely on the ability to distinguish a particular RNA structure, SimiR poses a new analytical challenge to the current methodologies.

CHAPTER VI

CONCLUSIONS

6.1 MALDI Matrix Cluster Ions as Internal Reference

The study aimed at developing an ion mobility mass spectrometry-based method for resolving isomeric modified/unmodified RNA biomarkers. Calibration in ion mobility has been an impedance in the sense that there lacks a universal calibrant that can be used across different platforms and in different laboratories. MALDI matrices are widely used across different ion mobility instrumentations. These matrices are in extension used across different laboratories and generate unique trendlines in the 2 D ion mobility plots. We therefore investigated the utility of these trendlines as internal reference to selected model molecular ions. The method has the potential of being applied on different platforms using MALDI as an ionization source. This can enable sharing of data across different laboratories and from different instrumentations. The initial models included an Auto Inducing Peptide (AIP) and Polyethylene Glycol (PEG). The results of this initial studies indicate a variety of the existing MALDI matrices do support the concept regardless of the ionization polarity of the compounds. Adopting this proposed reference method would promote both inter-laboratory and inter-instrumental sharing of mobility data. The routine use of intrinsic MALDI matrices as internal reference in ion mobility

will also aid in reduction of false positives in ion mobility measurements thus playing a role in improving the reliability of ion mobility instruments and their robustness.

6.2 Effects of Different Modes of Operations on Total Internal Energy of Ions in TWIMS

There are a variety of research articles describing studies conducted to investigate the heating of ions in ion mobility cell of the traveling wave mass spectrometry instruments including the Synapt G2 used in this study. However, none of these studies, to our knowledge has reported comparison of the internal energy of the ions as they transit the instrument from the ion source to the detector specifically with regard to the effect the heating has on the dissociation of ions in both operation modes i.e. TOF and Mobility TOF modes.

Using a number of different molecular structure ions, we have done a rather comprehensive comparison between the two modes of operation by performing CID in Trap and Transfer cells while keeping all other parameters constant. Results obtained from these experiments indicate that less CID energy is required to achieve the same percentage of dissociation in the Transfer cell when performing the experiments in TOF mode. We attribute this to the RF voltage heating of the ions as they traverse through the ion mobility cell which operates as an ion guide in TOF mode.

On the other hand, in ion mobility mode, you need more CID energy in the transfer cell to achieve the same percentage dissociation as in the trap cell. When performing CID energy in the transfer cell, the ions have traversed the ion mobility cell and collisional cooling is purported to have occurred such that the ions have less total internal energy

when in the Transfer cell. To investigate the role of the gases in the total internal energy of the ions, the gases were sequentially turned off and CID performed in the transfer cell. Results indicate that in the absence of either of the gases, total internal energy of the ions increases thus requiring less CID energy to achieve the same percentage dissociation. There were no software or instrument modifications/adjustments available to make the ion residence time both in the Trap and Transfer similar in order for the two collision cells % dissociation to be completely comparable, however, the wave velocity set as default for the Transfer cell was relatively low i.e. 150 m/s and would decrease the resident time compared to Trap's 250 m/s which by default has a prolonged trap time as ions accumulate in readiness for release into the IMS cell. The results obtained, and conclusion hereby drawn is with an assumption that the difference in residence time for the two cells was not significant enough to cause any significance difference observed in the probe ions used.

6.3 Extent of Isomerism in Human MicroRNA Biomarkers and Their Challenges Thereof

Recently, microRNAs have generated a lot of interest since their expression is associated with various types of diseases including different types of cancers. Their availability in body fluids including saliva has been touted as a possible minimally invasive diagnostic approach. Since they are small in size, they are expected to be similar in structure. However, the extent of their similarities had not been explored or reported. Our publication has shed light on how similar these important biomolecules can be and the challenges to both current and new analytical methods designed to analyze them. The

knowledge of the extent of isomerism and the number of SimiRs in the currently reported human microRNAs will assist researchers who aim to get a deep insight in their functions.

REFERENCES

1. Mwangi, J.; Chiu, N., High Percentage of Isomeric Human MicroRNA and Their Analytical Challenges. *Non-Coding RNA* **2016,** *2* (4), 13.

2. Kaufman, E. J.; Miska, E. A., The microRNAs of Caenorhabditis elegans. *Semin Cell Dev Biol* **2010,** *21* (7), 728-37.

3. Mou, G.; Wang, K.; Xu, D.; Zhou, G., Evaluation of three RT-qPCR-based miRNA detection methods using seven rice miRNAs. *Biosci Biotechnol Biochem* **2013,** *77* (6), 1349-53.

4. <Frequent deletions and down-regulation of micro- RNA genes miR15 and miR16 at 13q14 in chronic lymphocytic leukemia.pdf>.

5. Yin, J. Q.; Zhao, R. C.; Morris, K. V., Profiling microRNA expression with microarrays. *Trends Biotechnol* **2008,** *26* (2), 70-6.

6. Leshkowitz, D.; Horn-Saban, S.; Parmet, Y.; Feldmesser, E., Differences in microRNA detection levels are technology and sequence dependent. *RNA* **2013,** *19* (4), 527-38.

7. Machnicka, M. A.; Milanowska, K.; Osman Oglou, O.; Purta, E.; Kurkowska, M.; Olchowik, A.; Januszewski, W.; Kalinowski, S.; Dunin-Horkawicz, S.; Rother, K. M.; Helm, M.; Bujnicki, J. M.; Grosjean, H., MODOMICS: a database of RNA modification pathways--2013 update. *Nucleic Acids Res* **2013,** *41* (Database issue), D262-7.

8. Kellner, S.; Burhenne, J.; Helm, M., Detection of RNA modifications. *RNA Biology* **2014,** *7* (2), 237-247.

9. Ofengand, J.; Del Campo, M.; Kaya, Y., Mapping pseudouridines in RNA molecules. *Methods* **2001,** *25* (3), 365-73.

10. Basanta-Sanchez, M.; Temple, S.; Ansari, S. A.; D'Amico, A.; Agris, P. F., Attomole quantification and global profile of RNA modifications: Epitranscriptome of human neural stem cells. *Nucleic Acids Res* **2016,** *44* (3), e26.

11. Fawcett, K. A.; Barroso, I., The genetics of obesity: FTO leads the way. *Trends Genet* **2010,** *26* (6), 266-74.

12. Dominissini, D.; Moshitch-Moshkovitz, S.; Schwartz, S.; Salmon-Divon, M.; Ungar, L.; Osenberg, S.; Cesarkas, K.; Jacob-Hirsch, J.; Amariglio, N.; Kupiec, M.; Sorek, R.; Rechavi, G., Topology of the human and mouse m6A RNA methylomes revealed by m6A-seq. *Nature* **2012,** *485* (7397), 201-6.

13. Willmann, L.; Erbes, T.; Krieger, S.; Trafkowski, J.; Rodamer, M.; Kammerer, B., Metabolome analysis via comprehensive two-dimensional liquid chromatography: identification of modified nucleosides from RNA metabolism. *Anal Bioanal Chem* **2015,** *407* (13), 3555-66.

14. Fu, Y.; Dominissini, D.; Rechavi, G.; He, C., Gene expression regulation mediated through reversible m(6)A RNA methylation. *Nat Rev Genet* **2014,** *15* (5), 293-306.

15. Nicholson, D. A. T. a. N. H., <Sequencing RNA by a combination of exonuclease digestion and uridine specific chemical cleavage using MALDI-TOF.pdf>. *Nucleic Acids Research* **1998,** *26*, 446–451.

16. Takebayashi, K.; Hirose, K.; Izumi, Y.; Bamba, T.; Fukusaki, E., Application of ion mobility-mass spectrometry to microRNA analysis. *J Biosci Bioeng* **2013,** *115* (3), 332-8.

17. Dwivedi, P.; Puzon, G.; Tam, M.; Langlais, D.; Jackson, S.; Kaplan, K.; Siems, W. F.; Schultz, A. J.; Xun, L.; Woods, A.; Hill, H. H., Jr., Metabolic profiling of Escherichia coli by ion mobility-mass spectrometry with MALDI ion source. *J Mass Spectrom* **2010,** *45* (12), 1383-93.

18. Hofmann, J.; Hahm, H. S.; Seeberger, P. H.; Pagel, K., Identification of carbohydrate anomers using ion mobility-mass spectrometry. *Nature* **2015,** *526* (7572), 241-4.

19. Li, H.; Bendiak, B.; Siems, W. F.; Gang, D. R.; Hill, H. H., Jr., Determining the isomeric heterogeneity of neutral oligosaccharide-alditols of bovine submaxillary mucin using negative ion traveling wave ion mobility mass spectrometry. *Anal Chem* **2015,** *87* (4), 2228-35.

20. Jeanne Dit Fouque, K.; Afonso, C.; Zirah, S.; Hegemann, J. D.; Zimmermann, M.; Marahiel, M. A.; Rebuffat, S.; Lavanant, H., Ion mobility-mass spectrometry of lasso peptides: signature of a rotaxane topology. *Anal Chem* **2015,** *87* (2), 1166-72.

21. Allen, S. J.; Giles, K.; Gilbert, T.; Bush, M. F., Ion mobility mass spectrometry of peptide, protein, and protein complex ions using a radio-frequency confining drift cell. *Analyst* **2016,** *141* (3), 884-91.

22. Leijdekkers, A. G.; Huang, J. H.; Bakx, E. J.; Gruppen, H.; Schols, H. A., Identification of novel isomeric pectic oligosaccharides using hydrophilic interaction chromatography coupled to traveling-wave ion mobility mass spectrometry. *Carbohydr Res* **2015,** *404*, 1-8.

23. Laakia, J.; Kauppila, T. J.; Adamov, A.; Sysoev, A. A.; Kotiaho, T., Separation of isomeric amines with ion mobility spectrometry. *Talanta* **2015,** *132*, 889-93.

24. Gerislioglu, S.; Adams, S. R.; Wesdemiotis, C., Characterization of singly and multiply PEGylated insulin isomers by reversed-phase ultra-performance liquid chromatography interfaced with ion mobility mass spectrometry. *Anal Chim Acta* **2018,** *1004*, 58-66.

25. Barroso, A.; Gimenez, E.; Konijnenberg, A.; Sancho, J.; Sanz-Nebot, V.; Sobott, F., Evaluation of ion mobility for the separation of glycoconjugate isomers due to different types of sialic acid linkage, at the intact glycoprotein, glycopeptide and glycan level. *J Proteomics* **2018,** *173*, 22-31.

26. <Naked Protein Conformations- Cytochrome c in the Gas Phase.pdf>.

27. May, J. C.; Goodwin, C. R.; Lareau, N. M.; Leaptrot, K. L.; Morris, C. B.; Kurulugama, R. T.; Mordehai, A.; Klein, C.; Barry, W.; Darland, E.; Overney, G.; Imatani, K.; Stafford, G. C.; Fjeldsted, J. C.; McLean, J. A., Conformational ordering of biomolecules in the gas phase: nitrogen collision cross sections measured on a prototype high resolution drift tube ion mobility-mass spectrometer. *Anal Chem* **2014,** *86* (4), 2107-

28. <Design of a new electrospray ion mobility mass spectrometer.pdf>.

29. <Differential Ion Mobility Spectrometry- Nonlinear Ion Transport and Fundamentals of FAIMS.pdf>.

30. Zhong, Y.; Hyung, S. J.; Ruotolo, B. T., Characterizing the resolution and accuracy of a second-generation traveling-wave ion mobility separator for biomolecular ions. *Analyst* **2011,** *136* (17), 3534-41.

31. Giles, K.; Pringle, S. D.; Worthington, K. R.; Little, D.; Wildgoose, J. L.; Bateman, R. H., Applications of a travelling wave-based radio-frequency-only stacked ring ion guide. *Rapid Commun Mass Spectrom* **2004,** *18* (20), 2401-14.

32. Giles, K.; Wildgoose, J. L.; Langridge, D. J.; Campuzano, I., A method for direct measurement of ion mobilities using a travelling wave ion guide. *International Journal of Mass Spectrometry* **2010,** *298* (1-3), 10-16.

33. Shvartsburg, A. A.; Smith, R. D., Fundamentals of traveling wave ion mobility spectrometry. *Anal Chem* **2008,** *80* (24), 9689-99.

34. D'Atri, V.; Causon, T.; Hernandez-Alba, O.; Mutabazi, A.; Veuthey, J. L.; Cianferani, S.; Guillarme, D., Adding a new separation dimension to MS and LC-MS: What is the utility of ion mobility spectrometry? *J Sep Sci* **2018,** *41* (1), 20-67.

35. Forsythe, J. G.; Petrov, A. S.; Walker, C. A.; Allen, S. J.; Pellissier, J. S.; Bush, M. F.; Hud, N. V.; Fernandez, F. M., Collision cross section calibrants for negative ion mode traveling wave ion mobility-mass spectrometry. *Analyst* **2015,** *140* (20), 6853-61.

36. Ruotolo, B. T.; Benesch, J. L.; Sandercock, A. M.; Hyung, S. J.; Robinson, C. V., Ion mobility-mass spectrometry analysis of large protein complexes. *Nat Protoc* **2008,** *3* (7), 1139-52.

37. Marchand, A.; Livet, S.; Rosu, F.; Gabelica, V., Drift Tube Ion Mobility: How to Reconstruct Collision Cross Section Distributions from Arrival Time Distributions? *Anal Chem* **2017,** *89* (23), 12674-12681.

38. Lippens, J. L.; Ranganathan, S. V.; D'Esposito, R. J.; Fabris, D., Modular calibrant sets for the structural analysis of nucleic acids by ion mobility spectrometry mass spectrometry. *Analyst* **2016,** *141* (13), 4084-99.

39. Hines, K. M.; Ross, D. H.; Davidson, K. L.; Bush, M. F.; Xu, L., Large-Scale Structural Characterization of Drug and Drug-Like Compounds by High-Throughput Ion Mobility-Mass Spectrometry. *Anal Chem* **2017,** *89* (17), 9023-9030.

40. <Polymers for Traveling Wave Ion Mobility Spectrometry Calibration.pdf>.

41. Hines, K. M.; May, J. C.; McLean, J. A.; Xu, L., Evaluation of Collision Cross Section Calibrants for Structural Analysis of Lipids by Traveling Wave Ion Mobility-Mass Spectrometry. *Anal Chem* **2016,** *88* (14), 7329-36.

42. Kaur-Atwal, G.; O'Connor, G.; Aksenov, A. A.; Bocos-Bintintan, V.; Paul Thomas, C. L.; Creaser, C. S., Chemical standards for ion mobility spectrometry: a review. *International Journal for Ion Mobility Spectrometry* **2009,** *12* (1), 1-14.

43. Hillenkamp, M. K. a. F., Laser Desorption Ionization of Proteins with Molecular Masses Exceeding 10 000 Daltons. *Anal. Chem.* **1988,** (60), 2299-2301.

44. Chang, W. C.; Huang, L. C.; Wang, Y. S.; Peng, W. P.; Chang, H. C.; Hsu, N. Y.; Yang, W. B.; Chen, C. H., Matrix-assisted laser desorption/ionization (MALDI) mechanism revisited. *Anal Chim Acta* **2007,** *582* (1), 1-9.

45. <MALDI-Ion Mobility Separation-Mass Spectrometry Imaging of Glucose-regulated protein 78kDa.pdf>.

46. <MALDI imaging mass spectrometry of N-linked glycans on formalin-fixed paraffin-embedded murine kidney.pdf.pdf>.

47. <Identification of lipopeptide isoforms by MALDI-TOF-MS-MS based on the simultaneous RP-HPLC.pdf.pdf>.

48. al, B. e., <Fast urinary screening of oligosaccharidoses by MALDI-TOF-TOF mass spectrometry.pdf>. *Orphanet Journal of Rare Diseases* **2014,** *9* (19).

49. Nishikaze, T.; Kawabata, S.; Tanaka, K., In-depth structural characterization of N-linked glycopeptides using complete derivatization for carboxyl groups followed by positive- and negative-ion tandem mass spectrometry. *Anal Chem* **2014,** *86* (11), 5360-9.

50. <Role of photoionization and photochemistry in ionization processes of organic molecules and relevance for matrix-assisted laser desorption lonization mass spectrometry - Ehring - 1992 - Journal of Mass Spectrometry - Wiley Online Library.pdf>.

51. <Localization of Analyte Molecules in MALDI Preparations by Confocal Laser Scanning Microscopy.pdf>.

52. Bergman, N.; Shevchenko, D.; Bergquist, J., Approaches for the analysis of low molecular weight compounds with laser desorption/ionization techniques and mass spectrometry. *Anal Bioanal Chem* **2014,** *406* (1), 49-61.

53. Jiao, J.; Zhang, Y.; Yang, P.; Lu, H., Hydrazinonicotinic acid as a novel matrix for highly sensitive and selective MALDI-MS analysis of oligosaccharides. *Analyst* **2015,** *140* (1), 156-61.

54. Verbeck, B. L. W. a. G. F., Soft-Landing Ion Mobility of Silver Clusters for Small-Molecule Matrix-Assisted Laser Desorption Ionization Mass Spectrometry and Imaging of Latent Fingerprints. *Anal. Chem.* **2014,** (86), 8114−8120.

55. Kaplan, K.; Jackson, S.; Dwivedi, P.; Davidson, W. S.; Yang, Q.; Tso, P.; Siems, W.; Woods, A.; Hill, H. H., Monitoring dynamic changes in lymph metabolome of fasting and fed rats by matrix-assisted laser desorption/ionization-ion mobility mass spectrometry (MALDI-IMMS). *International Journal for Ion Mobility Spectrometry* **2012,** *16* (3), 177-184.

56. Schultz, M. U. T. E. J. K. K. J. G. K. F. M. G. a. J. A., Lipid/Peptide/Nucleotide Separation with MALDI-Ion Mobility-TOF MS. *Analytical Chemistry* **2004,** *76* (8), 2187-2195.

57. Campbell, J. L.; Le Blanc, J. C.; Kibbey, R. G., Differential mobility spectrometry: a valuable technology for analyzing challenging biological samples. *Bioanalysis* **2015,** *7* (7), 853-6.

58. Fernandez-Lima, F.; Kaplan, D. A.; Suetering, J.; Park, M. A., Gas-phase separation using a trapped ion mobility spectrometer. *Int J Ion Mobil Spectrom* **2011,** *14* (2-3).

59. Morsa, D.; Gabelica, V.; De Pauw, E., Effective temperature of ions in traveling wave ion mobility spectrometry. *Anal Chem* **2011,** *83* (14), 5775-82.

60. Merenbloom, S. I.; Flick, T. G.; Williams, E. R., How hot are your ions in TWAVE ion mobility spectrometry? *J Am Soc Mass Spectrom* **2012,** *23* (3), 553-62.

61. Cantara, W. A.; Crain, P. F.; Rozenski, J.; McCloskey, J. A.; Harris, K. A.; Zhang, X.; Vendeix, F. A.; Fabris, D.; Agris, P. F., The RNA Modification Database, RNAMDB: 2011 update. *Nucleic Acids Res* **2011,** *39* (Database issue), D195-201.

62. Glenn R. Bjork, J. U. E., Claes E.D. Gustafsson, Tord G. Hagervall, Yvonne H. Johnson, and P. Mikael Willkstom, Transfer RNA modification. *Ann. Rev. Biochem* **1987,** *56*, 263-287.

63. Gray, D. H. P. a. M. W., Chapter 16 Editing of tRNA. *ASMS press* **1998**.

64. Wetzel, C.; Limbach, P. A., Mass spectrometry of modified RNAs: recent developments. *Analyst* **2016,** *141* (1), 16-23.

65. Wendy V. Gilbert, T. A. B., 1, Cassandra Schaening,, Messenger RNA modifications- Form, distribution, and function.pdf. *SIGNALS IN RNA* **2016**.

66. Shelton, S. B.; Reinsborough, C.; Xhemalce, B., Who Watches the Watchmen: Roles of RNA Modifications in the RNA Interference Pathway. *PLoS Genet* **2016,** *12* (7), e1006139.

67. Squires, J. E.; Patel, H. R.; Nousch, M.; Sibbritt, T.; Humphreys, D. T.; Parker, B. J.; Suter, C. M.; Preiss, T., Widespread occurrence of 5-methylcytosine in human coding and non-coding RNA. *Nucleic Acids Res* **2012,** *40* (11), 5023-33.

68. Xhemalce, B.; Robson, S. C.; Kouzarides, T., Human RNA methyltransferase BCDIN3D regulates microRNA processing. *Cell* **2012,** *151* (2), 278-88.

69. Helm, M., Post-transcriptional nucleotide modification and alternative folding of RNA. *Nucleic Acids Res* **2006,** *34* (2), 721-33.

70. Kozomara, A.; Griffiths-Jones, S., miRBase: annotating high confidence microRNAs using deep sequencing data. *Nucleic Acids Res* **2014,** *42* (Database issue), D68-73.

71. Kozomara, A.; Griffiths-Jones, S., miRBase: integrating microRNA annotation and deep-sequencing data. *Nucleic Acids Res* **2011,** *39* (Database issue), D152-7.

72. Griffiths-Jones, S.; Saini, H. K.; van Dongen, S.; Enright, A. J., miRBase: tools for microRNA genomics. *Nucleic Acids Res* **2008,** *36* (Database issue), D154-8.

73. Griffiths-Jones, S.; Grocock, R. J.; van Dongen, S.; Bateman, A.; Enright, A. J., miRBase: microRNA sequences, targets and gene nomenclature. *Nucleic Acids Res* **2006,** *34* (Database issue), D140-4.

74. Asangani, I. A.; Rasheed, S. A.; Nikolova, D. A.; Leupold, J. H.; Colburn, N. H.; Post, S.; Allgayer, H., MicroRNA-21 (miR-21) post-transcriptionally downregulates tumor suppressor Pdcd4 and stimulates invasion, intravasation and metastasis in colorectal cancer. *Oncogene* **2008,** *27* (15), 2128-36.

75. Braconi, C.; Kogure, T.; Valeri, N.; Huang, N.; Nuovo, G.; Costinean, S.; Negrini, M.; Miotto, E.; Croce, C. M.; Patel, T., microRNA-29 can regulate expression of the long non-coding RNA gene MEG3 in hepatocellular cancer. *Oncogene* **2011,** *30* (47), 4750-6.

76. Liu, X.; Park, J. K.; Jiang, F.; Liu, Y.; McKearin, D.; Liu, Q., Dicer-1, but not Loquacious, is critical for assembly of miRNA-induced silencing complexes. *RNA* **2007,** *13* (12), 2324-9.

77. Doerks, T.; Copley, R. R.; Schultz, J.; Ponting, C. P.; Bork, P., Systematic identification of novel protein domain families associated with nuclear functions. *Genome Res* **2002,** *12* (1), 47-56.

78. Mlcochova, H.; Hezova, R.; Stanik, M.; Slaby, O., Urine microRNAs as potential noninvasive biomarkers in urologic cancers. *Urol Oncol* **2014,** *32* (1), 41 e1-9.

79. Scott Shell, S.-M. P., Amir Reza Radjabi, Robert Schickel, Emily O. Kistner, David A. Jewell§, Christine Feig, Ernst Lengyel, and Marcus E. Peter, Let-7 expression defines two differentiation stages of cancer.pdf. *PNAS* **2007,** *104* (27), 11400-11405.

80. Lu, L.; Katsaros, D.; de la Longrais, I. A.; Sochirca, O.; Yu, H., Hypermethylation of let-7a-3 in epithelial ovarian cancer is associated with low insulin-like growth factor-II expression and favorable prognosis. *Cancer Res* **2007,** *67* (21), 10117-22.

81. Heneghan, H. M.; Miller, N.; Lowery, A. J.; Sweeney, K. J.; Newell, J.; Kerin, M. J., Circulating microRNAs as novel minimally invasive biomarkers for breast cancer. *Ann Surg* **2010,** *251* (3), 499-505.

82. Yang, Y.; Xiao, L.; Li, J.; Kanwar, Y. S.; Liu, F.; Sun, L., Urine miRNAs: potential biomarkers for monitoring progression of early stages of diabetic nephropathy. *Med Hypotheses* **2013,** *81* (2), 274-8.

83. eggy S. Eis, W. T., Liping Sun, Amy Chadburn, Zongdong Li, Mario F. Gomez, Elsebet Lund, and James E. Dahlberg, Accumaulation of miR-155 and BIC RNA in human B cell lymphomas.pdf. *PNAS no. 10 3627–3632* **2005,** *vol. 102* (10), 3627-3632.

84. Bartels, C. L.; Tsongalis, G. J., MicroRNAs: novel biomarkers for human cancer. *Clin Chem* **2009,** *55* (4), 623-31.

85. Janssen, H. L.; Reesink, H. W.; Lawitz, E. J.; Zeuzem, S.; Rodriguez-Torres, M.; Patel, K.; van der Meer, A. J.; Patick, A. K.; Chen, A.; Zhou, Y.; Persson, R.; King, B. D.; Kauppinen, S.; Levin, A. A.; Hodges, M. R., Treatment of HCV infection by targeting microRNA. *N Engl J Med* **2013,** *368* (18), 1685-94.

86. Piehl, F.; Jagodic, M., MicroRNAs as promising novel biomarkers and potential drug targets for inflammatory neurological diseases. *J Neurol Sci* **2015,** *356* (1-2), 3-4.

87. &, R. W. F. Y. Q. Z. T. S. G. T. W. C. Y. Z.; Liu, B. L. X. Z. J., MicroRNA-148b is a potential prognostic biomarker and predictor of response to radiotherapy in non-small-cell lung cancer.pdf. *Physiological Biochemistry* **2016,** *72,* 337–343.

88. Teplyuk, N. M.; Uhlmann, E. J.; Gabriely, G.; Volfovsky, N.; Wang, Y.; Teng, J.; Karmali, P.; Marcusson, E.; Peter, M.; Mohan, A.; Kraytsberg, Y.; Cialic, R.; Chiocca, E. A.; Godlewski, J.; Tannous, B.; Krichevsky, A. M., Therapeutic potential of targeting microRNA-10b in established intracranial glioblastoma: first steps toward the clinic. *EMBO Mol Med* **2016,** *8* (3), 268-87.

89. Jingsheng, S.; Yibing, W.; Jun, X.; Siqun, W.; Jianguo, W.; Feiyan, C.; Gangyong, H.; Jie, C., MicroRNAs are potential prognostic and therapeutic targets in diabetic osteoarthritis. *J Bone Miner Metab* **2015,** *33* (1), 1-8.

90. Kalinowski, F. C.; Brown, R. A.; Ganda, C.; Giles, K. M.; Epis, M. R.; Horsham, J.; Leedman, P. J., microRNA-7: a tumor suppressor miRNA with therapeutic potential. *Int J Biochem Cell Biol* **2014,** *54*, 312-7.

91. Hunt, E. A.; Broyles, D.; Head, T.; Deo, S. K., MicroRNA Detection: Current Technology and Research Strategies. *Annu Rev Anal Chem (Palo Alto Calif)* **2015,** *8*, 217-37.

92. Pall, G. S.; Codony-Servat, C.; Byrne, J.; Ritchie, L.; Hamilton, A., Carbodiimide-mediated cross-linking of RNA to nylon membranes improves the detection of siRNA, miRNA and piRNA by northern blot. *Nucleic Acids Res* **2007,** *35* (8), e60.

93. Valoczi, A.; Hornyik, C.; Varga, N.; Burgyan, J.; Kauppinen, S.; Havelda, Z., Sensitive and specific detection of microRNAs by northern blot analysis using LNA-modified oligonucleotide probes. *Nucleic Acids Res* **2004,** *32* (22), e175.

94. Times, P. L., Old and New Ways to RNA .pdf. *Labs* **2012**, 52-61.

95. Agnieszka podolska, B. K., Thomas Litman, Marete Fredholm and Susanna Cirera, How the RNA isolation method can a ect microRNA microarray results. *Acta Biochemica polonica* **2011,** *58* (14883).

96. Morin, R. D.; O'Connor, M. D.; Griffith, M.; Kuchenbauer, F.; Delaney, A.; Prabhu, A. L.; Zhao, Y.; McDonald, H.; Zeng, T.; Hirst, M.; Eaves, C. J.; Marra, M. A., Application of massively parallel sequencing to microRNA profiling and discovery in human embryonic stem cells. *Genome Res* **2008,** *18* (4), 610-21.

97. Mirlinda Biba1, B. M., Christopher J. Welch, and Joe P. Foley,, Liquid Chromatography methods of separation of.pdf. *LC.GC solutions for separation scientists* **2014,** *online version*.

98. Jiang, Q.; Wang, Y.; Hao, Y.; Juan, L.; Teng, M.; Zhang, X.; Li, M.; Wang, G.; Liu, Y., miR2Disease: a manually curated database for microRNA deregulation in human disease. *Nucleic Acids Res* **2009,** *37* (Database issue), D98-104.